

## Static and dynamic properties of the $(\text{Fe}_x\text{Cr}_{1-x})_{75}\text{P}_{15}\text{C}_{10}$ reentrant-spin-glass amorphous alloy

Ph. Mangin, D. Boumazouza, and B. George

*Laboratoire de Physique du Solide, Unité Associée No. 155 du Centre National de la Recherche Scientifique, Université de Nancy-I, Boîte Postale 239, 54506 Vandoeuvre les Nancy CEDEX, France*

J. J. Rhyne and R. W. Erwin

*National Institute of Standards and Technology, Gaithersburg, Maryland 20899*

(Received 3 April 1989)

The reentrant-spin-glass behavior for members of the amorphous  $(\text{Fe}_x\text{Cr}_{1-x})_{75}\text{P}_{15}\text{C}_{10}$  and crystalline  $\text{Fe}_x\text{Cr}_{1-x}$  systems are found to be similar when the  $T_C$ 's are the same. This suggests some relationship between the width of the exchange distribution and the average exchange. We have constructed a phase diagram for these systems by combining Mössbauer, magnetization, and neutron scattering techniques. The ferromagnetic transitions appear conventional in all of these techniques. We assign three characteristic temperatures to the reentrant-spin-glass behavior. The highest temperature,  $T^*$ , corresponds to the first appearance of anomalies in the spin-wave dynamics and may also be related to the canting transition. The middle temperature,  $T_1$ , indicates the maximum in the zero-field-cooled magnetization, and also the approximate first appearance of anomalous small-angle neutron scattering. The magnetic structural changes are most pronounced below the lowest characteristic temperature,  $T_2$ , where strong irreversibilities occur in the magnetization and the small-angle neutron scattering becomes sufficiently intense that the correlation length appears to decrease. We make a rough correspondence with the phase diagram proposed by Gabay and Toulouse.

### I. INTRODUCTION

Competing interactions are known to be at the origin of spin-glass phenomena. Ferromagnetic and antiferromagnetic exchange interactions present in appropriate proportion cause frustration and consequently spin-glass behavior. In dilute alloys, competing interactions result from the oscillating long-distance behavior of the RKKY interactions and from the distribution of the distances between magnetic impurities.<sup>1</sup> The spin-glass behavior resulting from the competing interactions has been widely studied and is referred to as canonical. A peak is exhibited in the low-field ac susceptibility at a temperature  $T_G$ , and irreversible magnetic behavior occurs below this temperature. In addition, scaling laws are satisfied due to the  $1/r^3$  dependence of the interactions.<sup>2</sup>

Competing interactions can also be present in concentrated alloys with short-range ferromagnetic and antiferromagnetic exchange.<sup>1</sup> In crystalline alloys such as Fe-Cr, the Fe-Fe interactions are ferromagnetic and the Cr-Fe interactions are antiferromagnetic. The chemical disorder of the alloy then plays an essential part in producing spin frustration. In amorphous alloys such as  $(\text{Fe}_x\text{Ni}_{1-x})\text{-P-B-Al}$  (Ref. 3) the nearest-neighbor exchange interactions can be of either sign due to the distribution of interatomic distances, and again leads to frustrated spin couplings. Finally, in amorphous alloys such as  $(\text{Fe}_x\text{Cr}_{1-x})\text{-P-C}$  or  $(\text{Fe}_x\text{Cr}_{1-x})\text{-P-B-Al}$  the chemical (site) disorder of the iron and chromium or iron and manganese adds to the topological disorder and leads to a larger randomization of the exchange interactions.

Theoretical studies based on randomly distributed positive and negative exchange interactions predicted the occurrence of paramagnetic-spin-glass transitions.<sup>4-7</sup> In the paramagnetic phase the time-average spin is zero. In the spin glass the time averages are nonzero as in a ferromagnet but they are randomly orientated in space. The theory has in fact been extended to the case of nonidentical weights of the positive and negative interactions. Phase diagrams have been predicted as a function of the reduced parameter  $J_0/\Delta$  where  $J_0$  is the mean of the Gaussian distribution of exchange interactions and  $\Delta$  is its standard deviation. They show that with sufficient negative interactions  $J_0/\Delta < 1$ , a paramagnetic-spin-glass transition takes place. For  $J_0/\Delta > 1$ , the case in which the ferromagnetic interactions are dominant, the system undergoes a paramagnetic-ferromagnetic transition at a Curie temperature,  $T_C$ , and can exhibit a reentrant ferromagnetic-spin-glass like transition at a lower temperature. From the microscopic point of view, it means that the time average values of the spins are nonzero in the phase just below  $T_C$  and that the  $\langle \mathbf{S}_i \rangle$  are all parallel (within a domain). At low temperature, when the system undergoes the ferromagnetic-spin-glass reentrant transition, the time-average value of every spin continues to be nonzero but the spins are no longer parallel—their configurational average value can be zero if all  $\langle \mathbf{S}_i \rangle$  components are randomly orientated or nonzero if at least one component is not randomly distributed. Heisenberg mean-field model calculations<sup>7</sup> suggest that there are two distinct changes below  $T_C$ . At  $T_{GT}$  each spin should begin to acquire random static moment

components without the loss of the ferromagnetic order parameter (mixed phase  $M1$ ) and at a low  $T$ , a crossover to a mixed phase  $M2$  having the same ordering as phase  $M1$  and in addition the spontaneous breaking of replica symmetry. A weakly irreversible to strongly irreversible behavior should occur (phase  $M2$ ).

Experimentally, the reentrant-spin-glass (RSG) phase has been observed by low-field magnetic measurements. Canella *et al.*<sup>8</sup> and Coles *et al.*<sup>9</sup> showed that in the  $\text{Fe}_x\text{Au}_{1-x}$  system, the ac susceptibility peak of the paramagnetic-spin-glass transition observed for  $x < 0.15$ , was replaced by a plateau for higher iron concentrations. The plateau has been interpreted as a demagnetization limited plateau occurring in a ferromagnetic phase. Two knees mark the temperature extremes of the plateau—the upper knee occurs at the paramagnetic-ferromagnetic transition and the lower knee indicates that the system is entering a non ferromagnetic state, with features similar to those of spin glasses.

The main characteristic of the RSG is the high degree of irreversibilities and the low-temperature drop in the zero-field-cooled low-field magnetization. This was studied by many authors, and in particular by Senoussi *et al.*,<sup>10,11</sup> Abdul-Razzaq and Kouvel<sup>12</sup> in the  $\text{Fe}_x\text{Au}_{1-x}$  and  $\text{Ni}_x\text{Mn}_{1-x}$  systems. They studied in detail the effect of the cooling field on the magnetization and on the hysteresis loop and concluded that the large irreversibilities of the zero-field-cooled samples are related to domains frozen during the cooling process and anisotropies. Their sizes would depend on the magneto-thermal history of the sample. According to Abdul-Razzaq and Kouvel,<sup>12</sup>  $\text{Ni}_{77}\text{Mn}_{23}$  samples cooled under a field larger than 2000 Oe act essentially as a single domain with an anisotropy axis along the cooling field. For lower cooling fields, the sample is subdivided into smaller domains with different anisotropy directions. Senoussi<sup>10</sup> suggests that, during the cooling of FeAu and NiMn alloys, “quasiferromagnetic domains” freeze in a Weiss-type molecular field. The latter behaves like a strong cooling field having the direction of the associated magnetic domain during cooling.

Strong irreversibilities and differences between field-cooled  $\sigma_{\text{FC}}$  and zero-field-cooled  $\sigma_{\text{ZFC}}$  magnetization are not the only features of the RSG. In many cases, a reversible decrease of  $\sigma_{\text{FC}}$  is observed at higher temperatures and is more pronounced near the spin-glass-ferromagnetic critical concentration.<sup>11,13</sup> This has been interpreted by Senoussi<sup>11</sup> as a reduction of the degree of long-range magnetic order and is not associated with the occurrence of strong irreversibilities. In an  $(\text{Fe}_x\text{Mn}_{1-x})_{75}\text{P}_{16}\text{B}_6\text{Al}_3$  amorphous alloy, Manheimer *et al.*<sup>13</sup> showed that this reversible part of the magnetization yields scaling behavior consistent with that expected from a second-order magnetic transition.

Deviations from standard ferromagnetic behavior also result in anomalous features in small-angle neutron scattering (SANS) experiments. By this technique, magnetic inhomogeneities can be studied at zero field. SANS has been carried out on crystalline  $\text{Fe}_x\text{Cr}_{1-x}$ ,<sup>14,15</sup>  $\text{Fe}_x\text{Au}_{1-x}$ ,<sup>16</sup> as well as on amorphous  $(\text{Fe}_x\text{Mn}_{1-x})_{75}\text{P}_{16}\text{B}_6\text{Al}_3$ ,<sup>17</sup>  $(\text{Fe}_x\text{Ni}_{1-x})_{75}\text{P}_{16}\text{B}_6\text{Al}_3$  (Ref. 3)

systems. All the data show unusual SANS behavior at low temperatures for alloys close to the multicritical spin-glass to paramagnetic-ferromagnetic point. Contrary to that expected from a standard ferromagnet, the scattering intensity increases (in some cases shows a maximum,<sup>16,17</sup> at low temperature especially for the lower  $q$  (scattering vector) values. The spin correlation lengths (see Sec. III) obtained from the scattering lineshapes have been studied as a function of temperature by Aeppli *et al.*,<sup>17</sup> and Erwin<sup>3</sup> in the  $(\text{Fe}_x\text{Mn}_{1-x})\text{-P-B-Al}$  and  $(\text{Fe}_x\text{Ni}_{1-x})\text{-P-B-Al}$  systems, respectively. It has been shown that the correlation length decreases at low temperature from a large value in the ferromagnetic temperature range. On the other hand, it has been shown that the SANS was strongly influenced by a magnetic field. An external field suppresses the largest part of the low- $T$ , low- $q$  SANS (Ref. 17a), which can then exhibit additional structure.<sup>18</sup> Removal of the field at low temperature shows that this contribution to the SANS depends on the thermal history of the sample.<sup>19</sup> This illustrates that the magnetic inhomogeneities can vary in size and density with field and temperature.

A third measurement indicating nonstandard ferromagnetic behavior at low temperature is that of the spin waves. Spin waves anomalies have been studied by Fincher *et al.*,<sup>15</sup> Shapiro *et al.*<sup>20</sup> in  $\text{Fe}_x\text{Cr}_{1-x}$ , Murani<sup>21</sup> in  $\text{Fe}_x\text{Au}_{1-x}$ , Hennion *et al.*<sup>22</sup> in the  $\text{Ni}_x\text{Mn}_{1-x}$  crystalline systems, and by Aeppli *et al.*<sup>17</sup> in  $(\text{Fe}_x\text{Mn}_{1-x})_{75}\text{-P-B-Al}$ , Lynn *et al.*<sup>23</sup> and Erwin *et al.*<sup>24</sup> in the  $(\text{Fe}_x\text{Ni}_{1-x})_{75}\text{-P-B-Al}$  amorphous alloys. The data obtained by these authors are very similar (see review by Rhyne<sup>25</sup>). They show that the stiffness and the width of the spin waves exhibit an anomalous behavior at low temperature attributed to the breakdown of ferromagnetic order (in some cases, however, contrasting anomalies have been observed at lower temperatures.<sup>22</sup> These techniques as well as others (e.g., Mössbauer spectroscopy<sup>26,27</sup> show that at low temperature these systems do not exhibit standard ferromagnetic behavior.

In this paper we report a systematic study of the magnetic properties of the  $(\text{Fe}_x\text{Cr}_{1-x})_{75}\text{P}_{15}\text{C}_{10}$  amorphous system in the concentration range in which RSG occurs. We performed low-field magnetization, SANS, spin-wave measurements and Mössbauer spectroscopy in an attempt to correlate the observed features of strong irreversibilities, maxima in  $\sigma_{\text{FC}}$ , anomalous SANS and spin wave damping.<sup>19,28,29</sup>

In Sec. II we report the magnetic measurements in fields up to 20 kOe and also in very low fields that allowed us to examine the different magnetic states. In Sec. III the SANS data are reported, in particular the correlation length as a function of temperature and field are compared to conventional ferromagnetic behavior. The inelastic scattering data are reported in Sec. IV, including the behavior of the spin-wave energy and energy width as a function of the temperature. Finally in Sec. V we discuss the collected data and present a synthesized view of the magnetic transitions in the samples from the paramagnetic phase to the spin-glass phase.

In addition, we correlate our results with data collected from the crystalline counterpart  $(\text{Fe}_x\text{Cr}_{1-x})$  base alloys

in their respective concentration range of reentrant-spin-glass phases. This system is one of the few opportunities to examine differences between the magnetic behavior of topologically disordered amorphous alloys and a crystalline but site disordered counterpart alloy.

## II. MAGNETIC MEASUREMENTS

### A. High-field studies

Chromium in both crystalline and amorphous  $\text{Fe}_x\text{Cr}_{1-x}$ -based alloys suppresses the Fe moment as has been discussed by Boliang *et al.*<sup>30</sup> from Mössbauer measurements on the  $(\text{Fe}_x\text{Cr}_{1-x})_{80}\text{B}_{20}$  system. According to these authors, hybridization of Cr and Fe 3d orbitals should be more effective in the amorphous structure than in the bcc crystals, so that the presence of chromium neighbors would have a greater effect on the local iron 3d density of states in an amorphous alloy.

Magnetization measurements in fields up to 20 kOe have been carried out on samples of composition between  $x=0.75$  and  $x=0.55$ . For the more iron-concentrated alloys ( $x=0.75, x=0.70$ ), the curves of  $\sigma$  versus  $H$  are characteristic of a ferromagnet and show essential saturation below 10 kOe. For the less concentrated samples ( $x < 0.62$ ), the behavior is closer to that of a superparamagnet. From these data, we deduced the saturation magnetization  $\sigma_{\text{sat}}$  by extrapolating  $\sigma$  to the  $1/H \rightarrow 0$  limit. This procedure is valid for the ferromagnetic samples  $x=0.70$  and  $x=0.75$  but very poor for  $x=0.55$ . As shown in Fig. 1,  $\sigma_{\text{sat}}$  extrapolates to  $2\mu_B$  for  $x=1$ , with a slope of  $3.6\mu_B/x$ . Such a linear behavior with a limit of  $2\mu_B$  has been observed in the  $0.9 < x < 1$  range in similar alloys,<sup>31</sup> but with a slightly higher slope. The average iron moment in crystalline  $\text{Fe}_x\text{Cr}_{1-x}$  alloys is practically linear also in the  $0.3 < x < 1$  range but with a smaller slope of  $2.45\mu_B/x$ .<sup>32</sup>

The temperature dependence of the magnetization measured at  $H=20$  kOe in the  $x=0.65$  sample (Fig. 2) shows a very long tail at high temperatures. As in many other amorphous samples,  $\text{Fe}_x\text{Pd}_{82-x}\text{Si}_{18}$  (Ref. 33) or  $(\text{Fe}_{0.2}\text{Ni}_{0.8})_{75}\text{P}_{16}\text{B}_6\text{Al}_3$  (Ref. 34) and other soft magnetic materials, no well-defined feature is evident in the isofield magnetization at the Curie temperature ( $T_C=84$  K). The susceptibility of these alloys in the paramagnetic phase is very large and no transition is observed except under very small fields.

### B. Low-field studies

We focus our attention on low-field magnetization measurements where the external field does not significantly mask the transitions from paramagnetism to ferromagnetism and from ferromagnetism to spin glass. In the low-field case however, we have to consider the effect of the demagnetization field inside the sample. If  $N$  is the demagnetization factor, the measured susceptibility  $\chi_m$  (or the measured magnetization  $\sigma_m$ ) does not correspond exactly to the intrinsic values  $\chi_i$  (and  $\sigma_i$ ). They are linked by the relations

$$1/\chi_m = 1/\chi_i + 1/(1/N) \quad \text{or} \quad 1/\sigma_m = 1/\sigma_i + 1/(H/N).$$

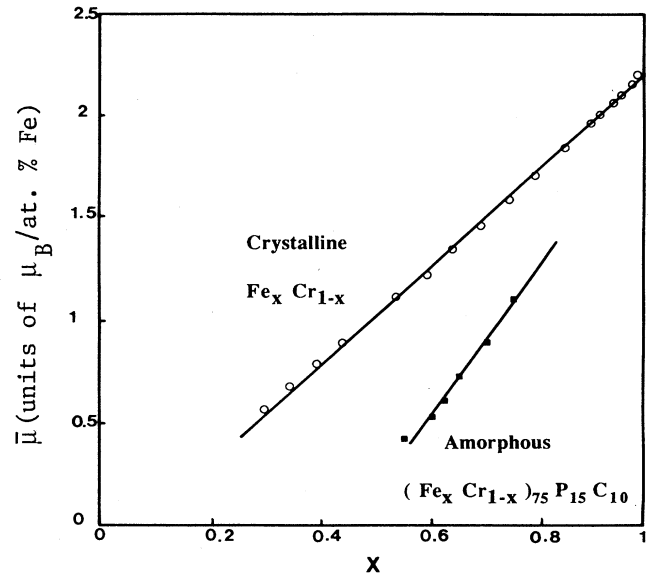


FIG. 1. Comparison between average saturation moment in crystalline  $\text{Fe}_x\text{Cr}_{1-x}$  ( $\odot$ ) (Ref. 32) and in amorphous  $(\text{Fe}_x\text{Cr}_{1-x})_{75}\text{P}_{15}\text{C}_{10}$  ( $\square$ ) (this work).

Thus if  $\sigma_i \ll H/N$  (large  $H$ , small  $N$ ) the measured magnetization  $\sigma_m$  does correspond to the intrinsic magnetization. But if  $\sigma_i \gg H/N$  (small  $H$ , large  $N$ ),  $\sigma_m$  is limited by the demagnetization plateau  $H/N$ . Therefore, to detect a sharp transition at  $T_C$  in the order parameter (or in  $\chi_i$ ) in going from paramagnetism to ferromagnetism, it is necessary to have  $H/N$  small. On the other hand, to observe small changes in the spontaneous magnetization, the plateau must be avoided, but at the same time  $H$  must be small enough to not smear the transition. To obtain a large value of  $H/N$  at small  $H$ , the field must be oriented parallel to the long dimension of the ribbons. Conversely to produce a plateau, it is necessary to apply the magnetic field perpendicular to the plane of the ribbons, or to apply a very low field in the plane (provided the thickness is not too small). In the measurements reported here several ribbons were stacked to get higher sensitivity.

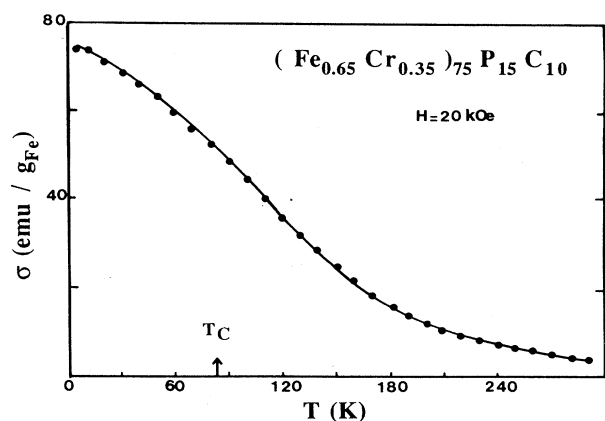


FIG. 2. Magnetization for  $H=20$  kOe in the  $(\text{Fe}_{0.65}\text{Cr}_{0.35})_{75}\text{P}_{15}\text{C}_{10}$  amorphous alloys.

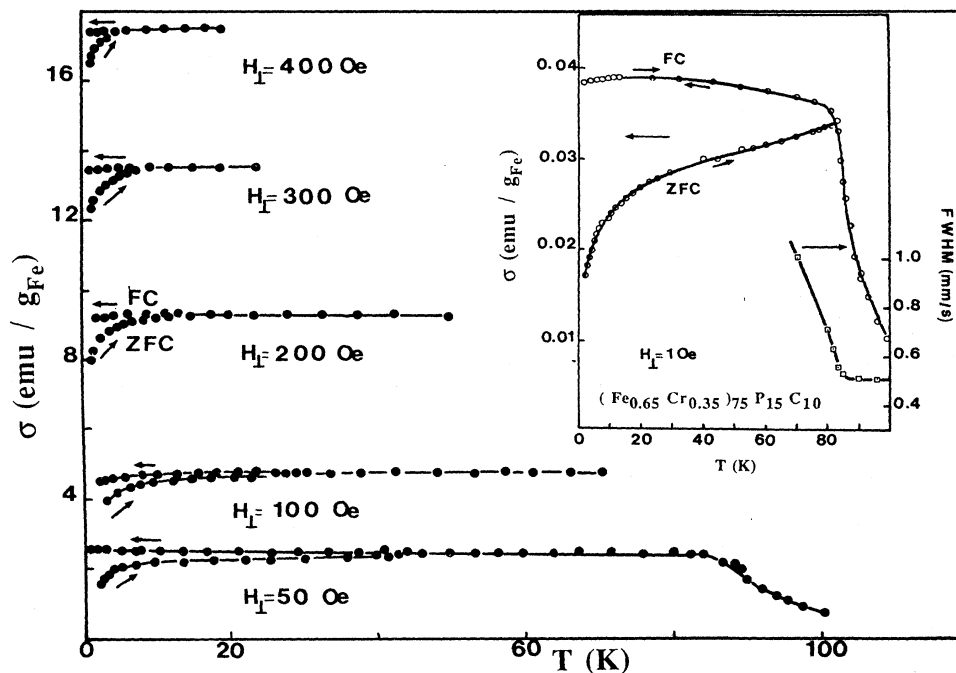


FIG. 3. Field-cooled  $\sigma_{FC}$  and zero-field-cooled  $\sigma_{ZFC}$  magnetization data collected from the  $(\text{Fe}_{0.65}\text{Cr}_{0.35})_{75}\text{P}_{15}\text{C}_{10}$  alloy in the perpendicular geometry. The inset shows  $\sigma_{FC}$  and  $\sigma_{ZFC}$  under 1 Oe ( $\odot$ ) and displays the full width at half maximum (FWHM) of the Mössbauer doublet near  $T_c$  ( $\square$ ).

1.  $(\text{Fe}_{0.65}\text{Cr}_{0.35})_{75}\text{P}_{15}\text{C}_{10}$

Figures 3 and 4 show zero-field-cooled (ZFC) and field-cooled (FC) magnetization data collected in perpendicular and parallel geometry. The overall magnetization

curve in the perpendicular geometry shows the behavior of a classical reentrant spin glass. The zero-field-cooled demagnetization plateau (proportional to  $H$ ) terminates in two knees, at the paramagnetic and spin-glass transitions. The upper knee of the plateau allows  $T_c$  to be

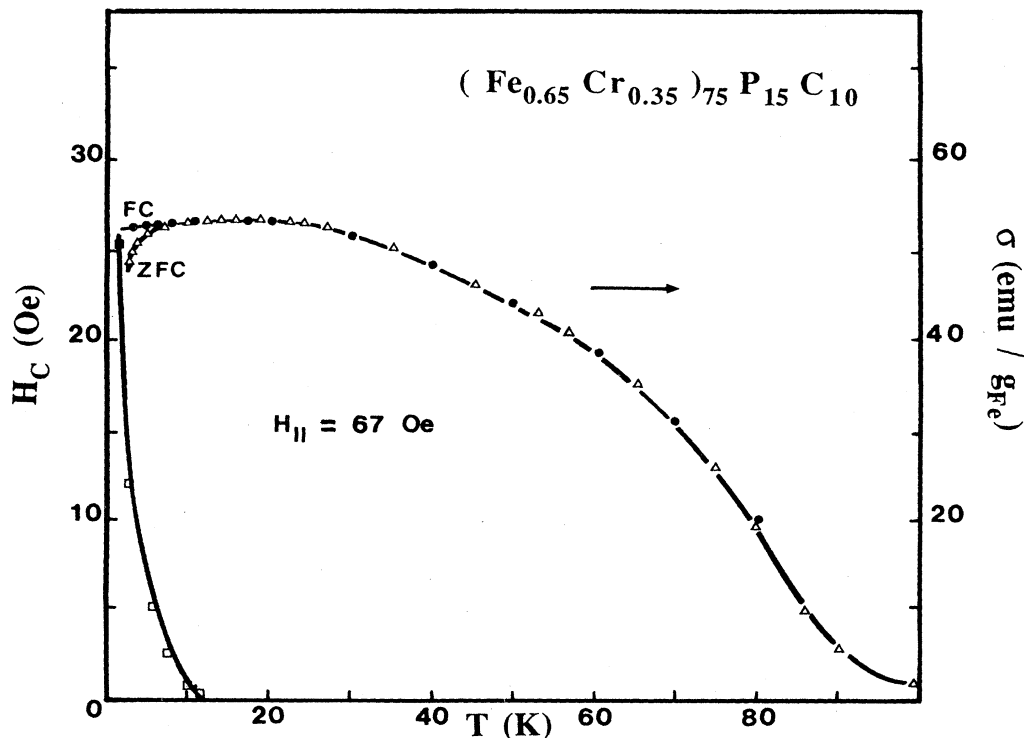


FIG. 4. Field-cooled and zero-field-cooled magnetization data collected from the  $(\text{Fe}_{0.65}\text{Cr}_{0.35})_{75}\text{P}_{15}\text{C}_{10}$  alloy in the parallel geometry. The coercive field  $H_c$  ( $\square$ ) is large in the temperature range in which  $\sigma_{FC}$  ( $\odot$ ) and  $\sigma_{ZFC}$  ( $\triangle$ ) are split.

determined with good accuracy. From the lowest-field demagnetization plateau ( $H_1 = 1$  Oe, Fig. 3 inset) the Curie temperature can be evaluated as  $84 \pm 2$  K. To verify that the upper edge of the plateau does correspond to the magnetic transition temperature, we performed absorption Mössbauer spectroscopy experiments in a 25-K temperature range around  $T_C$ . In this temperature range, the Mössbauer spectra are a doublet due mainly to the quadrupolar splitting. However, when we fit the doublet by two Lorentzians, we observe the width of the Lorentzians is constant above 84 K but increases significantly below this temperature, corresponding to the onset of a magnetic hyperfine field. Moreover below 84 K, the fit by a doublet becomes poorer and poorer. More precisely this means that the time average of the spins is zero (on the  $10^{-7}$  s scale) above 84 K.

The irreversibilities at very low field (Fig. 3) extend over the full temperature range to  $T_C$ . However, we can separate them into two parts: (1) the largest irreversibilities are independent of the applied field and occur below about 8 K, and (2) weak irreversibilities that occur above this temperature and are strongly dependent on the external field. In very low field small differences in  $\sigma_{FC}$  and  $\sigma_{ZFC}$  persist up to  $T_C$  (Fig. 3 inset) reflecting the hysteretic behavior of the magnetization. Due to the large demagnetizing field in the perpendicular geometry, small fields do not produce appreciable domain rotation.

In the parallel geometry, because of the small value of  $H/N$ , the Curie temperature cannot be determined accurately. What is interesting in this geometry is the increase of the field-cooled magnetization as the temperature is lowered and then its small reversible decrease below 20 K. As this field is large enough to remove domains, but not large enough to affect the intrinsic disorder, the measured magnetization is certainly close to the spontaneous magnetization. This behavior is not seen in a conventional ferromagnet, nor is a result of the demagnetization-limited plateau. It is similar to that observed by Senoussi<sup>11</sup> and Manheimer *et al.*<sup>13</sup>

In addition to the small  $\sigma_{FC}$  decrease below about 20 K, a significant difference is observed between  $\sigma_{FC}$  and  $\sigma_{ZFC}$  below 8 K. Only the large irreversibilities occurring in the perpendicular geometry are still present when the field is applied in the plane of the ribbons.

### 2. $(Fe_{0.62}Cr_{0.38})_{75}P_{15}C_{10}$

Figure 5 shows  $\sigma_{FC}$  and  $\sigma_{ZFC}$  for  $x=0.62$  in the parallel geometry under an external field of 4 Oe (a) and 28 Oe (b). With  $H_{ext} = 4$  Oe,  $H/N$  is small enough to give evidence of the demagnetization plateau. The upper knee is at about 50 K. It corresponds to the temperature below which a hyperfine field splitting is evident in the Mössbauer absorption lines. With  $H = 28$  Oe, the field-cooled parallel magnetization approximates the spontaneous magnetization and exhibits a better defined maximum at about 20 K. Between 30 and 40 K the magnetization curve flattens and falls below values that would be expected for the order parameter of a ferromagnet, and below 10-K strong irreversibilities occur for  $H = 28$  Oe as well as for  $H = 4$  Oe. Below 4 K, the 28 Oe external field

is insufficient to significantly perturb the zero-field-cooled state. As in the previous sample, small irreversibilities are also observed up to  $T_C$  when  $H/N$  is small.

### 3. $(Fe_{0.60}Cr_{0.40})_{75}P_{15}C_{10}$

In this sample a very small field is required to exhibit a demagnetization plateau in  $\sigma_{FC}$  (Fig. 6a). The upper knee of the plateau is observed at about 30 K which corresponds again to the onset of the hyperfine field. For higher fields [Fig. 6(b)],  $\sigma_{FC}$  exhibits a rounded maximum

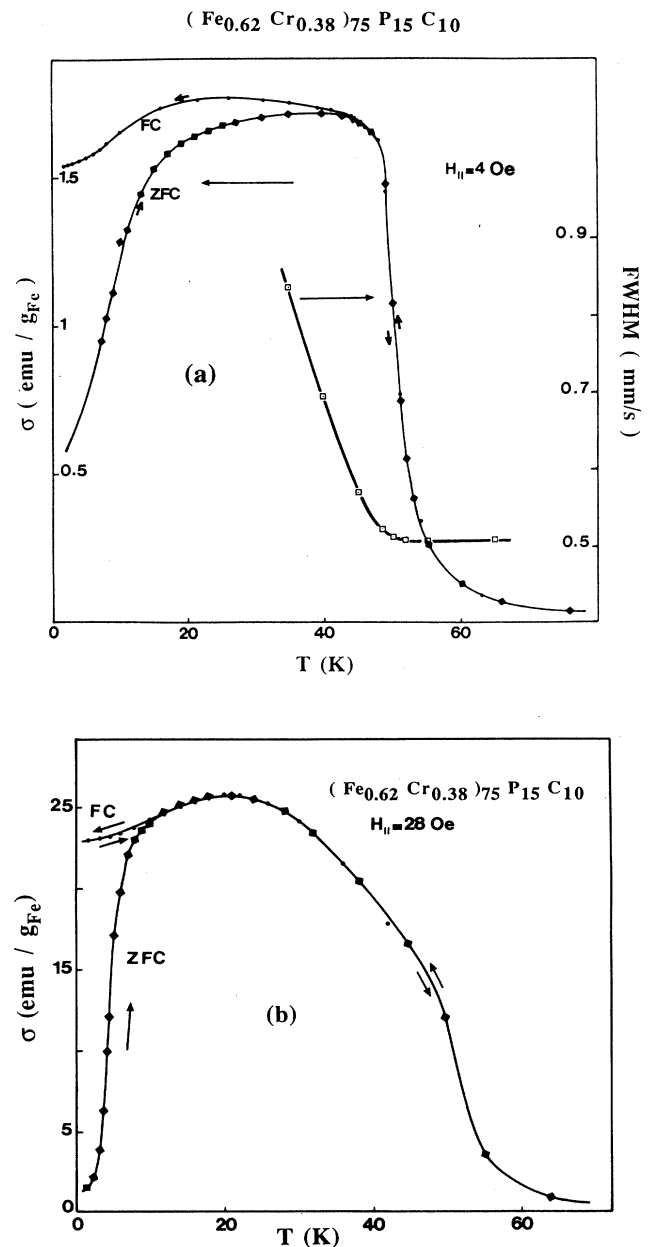


FIG. 5. Magnetization ( $\sigma$ ) and Mössbauer spectroscopy data (FWHM) ( $\square$ ) from the  $(Fe_{0.62}Cr_{0.38})_{75}P_{15}C_{10}$  amorphous alloys at 4 Oe (a) and at 28 Oe (b).

near 20 K and the regime of strong irreversibilities is below 15 K. For concentrations below  $x=0.6$ ,  $\sigma_{ZFC}$  becomes very small and shows a sharp peak like that in conventional spin glasses.

### C. Virgin curves and coercive fields

To get a better idea of the irreversibilities at low-temperature magnetization and hysteresis cycles have

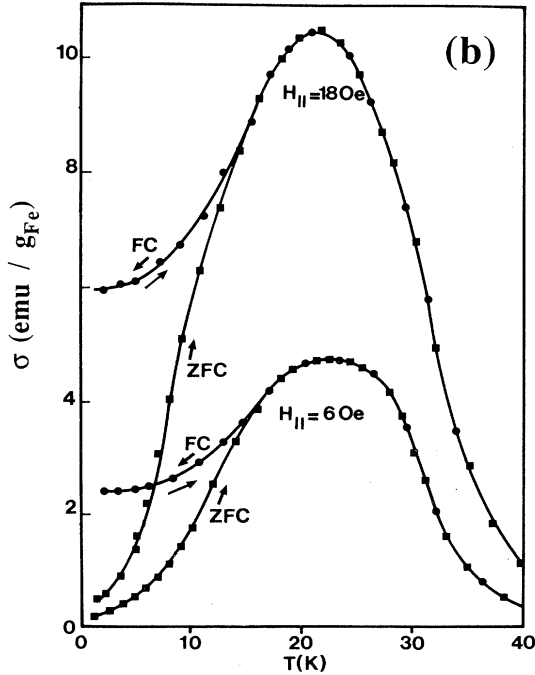
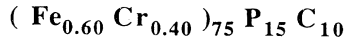
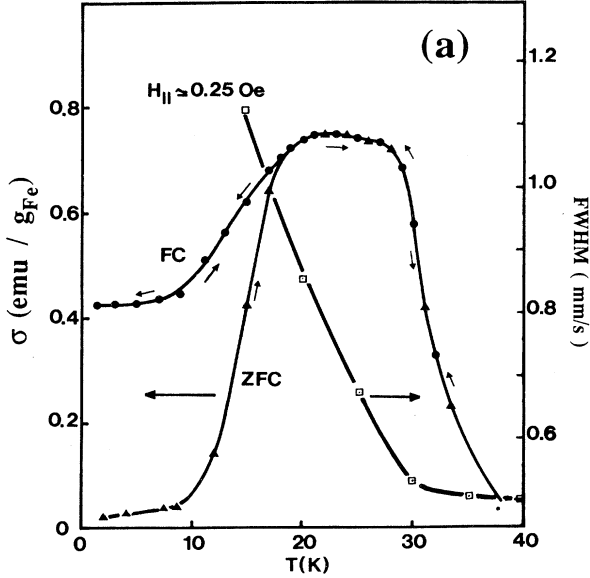
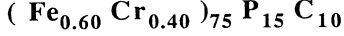


FIG. 6. Magnetization ( $\sigma$ ) and Mössbauer spectroscopy data (FWHM) ( $\square$ ) from the  $(\text{Fe}_{0.60}\text{Cr}_{0.40})_{75}\text{P}_{15}\text{C}_{10}$  amorphous alloys at 0.25 Oe (a) and 6 and 18 Oe (b).

been measured at 1.68 K after cooling the samples in zero field. The virgin curves of Fig. 7 show that below a field estimated at 15 Oe for  $x=0.65$ , 80 Oe for  $x=0.62$  and 150 Oe for  $x=0.60$ , the magnetization increases more slowly. As pointed out by Senoussi,<sup>11</sup> this is a field under which the domains remain relatively fixed. These fields are very close to the coercive fields as shown in the inset of Fig. 7. The coercive field in  $(\text{Fe}_{0.65}\text{Cr}_{0.35})_{15}\text{P}_{15}\text{C}_{10}$  becomes practically 0 above about 8–10 K (i.e., at about the temperature for which  $\sigma_{ZFC}$  become equal to  $\sigma_{FC}$ ) and below which strong irreversibilities occur.

## III. SMALL-ANGLE NEUTRON SCATTERING

### A. Background

The small-angle neutron scattering intensity (SANS) is directly proportional to the instantaneous spin-spin correlation function. It provides information on the spin correlation range when the experimental  $q$  (wave vector) range is appropriate. For a paramagnetic system at  $T \gg T_C$ , the instantaneous correlations between spins are very weak and the scattering is diffuse. As  $T$  comes closer to  $T_C$ , magnetic fluctuations take place and a snapshot of the spins show they follow instantaneously an Ornstein-Zernike law:<sup>35,36</sup>

$$\langle \mathbf{S}_i(0) \cdot \mathbf{S}_j(r) \rangle \simeq (1/r) e^{-r/\xi}.$$

The corresponding scattering law is a Lorentzian,

$$I(q) \simeq A / (\kappa^2 + q^2),$$

where  $\xi = 1/\kappa$  is the correlation length. As  $T \rightarrow T_C$ ,  $\kappa \rightarrow 0$  and the correlation length diverges. In simple mean-field theory,  $\kappa \propto (T - T_C)^\nu$  and  $\nu = \frac{1}{2}$ . In the paramagnetic phase, the time average of the spins  $\langle \mathbf{S}_i \rangle$  is zero and all the directions are equivalent. In a ferromagnetic phase, below  $T_C$ , the symmetry is broken. For every spin,

$$\langle S_i^z \rangle = m(T)/N \neq 0, \quad \langle S_i^x \rangle = \langle S_i^y \rangle = 0.$$

The order parameter  $m(T)$  increases as  $T$  decreases and two types of magnetic fluctuations appear: longitudinal fluctuations ( $\Delta S_i^z$ ) and transverse fluctuations ( $\Delta S_i^x, \Delta S_i^y$ ). Below  $T_C$ , it becomes necessary to differentiate between the longitudinal susceptibility and the transverse susceptibility, and the SANS cross section can be written as the sum of two Lorentzians:

$$I(q) = A_{\parallel} / (\kappa_{\parallel}^2 + q^2) + A_{\perp} / (\kappa_{\perp}^2 + q^2),$$

where in mean-field theory<sup>35,36</sup>

$$2A_{\parallel} = A_{\perp}, \quad \kappa_{\perp}^2 = 0, \quad \kappa_{\parallel}^2 \propto (T_C - T)^{2\nu},$$

$$\nu = \frac{1}{2}, \quad A_{\parallel} + A_{\perp} = A.$$

At  $T_C$  the occurrence of a transverse correlation function with  $\kappa_{\perp} = 0$  is the signature of the ferromagnetic phase and means that the perpendicular susceptibility is infinite. The limitation of the correlation length is then the size of the domains. Below  $T_C$  as the temperature is lowered, the longitudinal fluctuations decrease rapidly,  $\kappa_{\parallel}$

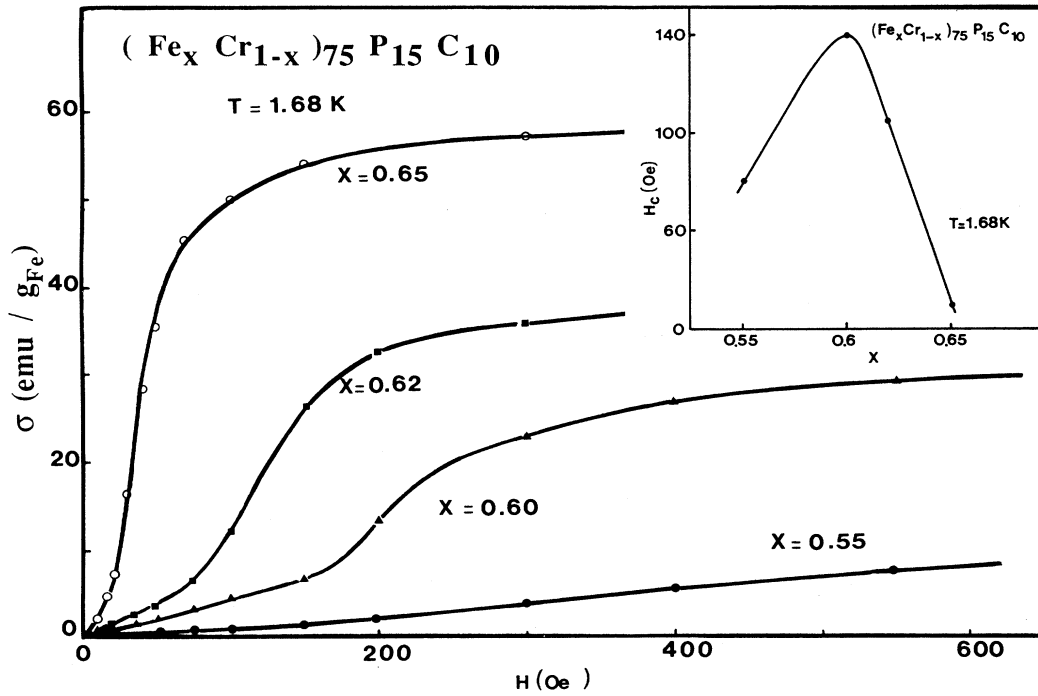


FIG. 7. Comparison of the virgin magnetization curves obtained from different alloys at 1.68 K. Inset displays the coercive field measured from the same samples.

becomes large, and the associated scattering is minimized. The transverse fluctuations (spin waves) follow the Bose thermal population factor, and this scattering also becomes less intense as  $T$  decreases.

In the reentrant-spin-glass phase, the above description is no longer valid because the time averaged spins  $\langle S_i \rangle$  are not all parallel. Two cases have to be considered:

(i) The misorientation of spins is nearly random from site to site so that the disordering gives rise to an incoherent scattering.

(ii) The spins or only their transverse components become misoriented but with special correlations that give rise to small angle neutron scattering.

In the latter case, the scattering law may not be of the Ornstein-Zernike form. For example if the disordering creates microdomains with relatively sharp walls between ordered regions, the scattering law will be of the Porod type,  $I \approx 1/q^4$ , for the larger  $q$  values. If the domains are random in size and shape the scattering law can be a Debye-type<sup>37</sup> Lorentzian squared in the small- $q$  regime ( $q$  approximately equal to the inverse of the size domain). For this case the overall scattering law has been written as a Lorentzian plus a Lorentzian squared:

$$I(q) = \bar{A}/(\kappa^2 + q^2) + \bar{B}/(\kappa^2 + q^2)^2.$$

Such an expression is often introduced for random field and random anisotropy systems.<sup>38,39</sup>

#### B. General features of SANS in the $(\text{Fe}_x \text{Cr}_{1-x})_{75} \text{P}_{15} \text{C}_{10}$ amorphous alloys

The general features of the SANS are displayed in Figs. 8 and 9. Figure 8(a) shows the variation of the intensity  $I$

normalized to 1 at  $T_C$ , collected at  $q = 0.04 \text{ \AA}^{-1}$ , as a function of the temperature for the four alloys studied in detail ( $x = 0.6, 0.62, 0.65, 0.70$ ). Figure 9 displays the intensities collected from the  $x = 0.70$  sample for three different  $q$  values. Figure 8(b) shows similar data to Fig. 8(a) but is for the  $\text{Fe}_x \text{Cr}_{1-x}$  crystalline counterpart alloy.<sup>15</sup> Two contributions to the intensity can be observed: the critical scattering (CS) which occurs near  $T_C$  and gives a well defined peak (except at very low  $q$ ), and the subcritical scattering (SS) which takes place at low temperature. As seen in Figs. 8 and 9 at a given  $q$  value, the SS becomes relatively more pronounced in alloys whose Curie temperature is lower. In a given alloy because of its higher- $q$  dependence, the SS is relatively larger for the smaller- $q$  values and masks the CS entirely for sufficiently small  $q$ .

Moreover, the comparison between data collected from the  $(\text{Fe}_x \text{Cr}_{1-x})_{75} \text{P}_{15} \text{C}_{10}$  amorphous system and from crystalline  $\text{Fe}_x \text{Cr}_{1-x}$ ,<sup>15,20</sup> shows that for the same scattering vector (e.g.,  $q = 0.04 \text{ \AA}^{-1}$ ), both the CS and the SS are of the same order of magnitude for alloys whose Curie temperatures are approximately the same.

#### C. Analysis of the data for $x = 0.70$ and $x = 0.65$

For all four alloys studied in this composition range, the inverse of the intensity as a function of  $q^2$  is quite linear above  $T_C$ . The straight lines obtained at the different temperatures are parallel and intersect the  $1/I$  axis closer to zero as  $T$  approaches  $T_C$ , indicating agreement with the Ornstein-Zernike (Lorentzian) law above  $T_C$ . Below  $T_C$ , the  $1/I$  versus  $q^2$  lines depart from paral-

lel. They exhibit a *downward* curvature at low  $q$ . At even lower temperatures,  $1/I$  versus  $q^2$  departs further from the linearity, but this time with a pronounced *upward* curvature.

In order of decreasing temperature, the best fits to the data were (1) by a single Lorentzian, (2) by the sum of two Lorentzians and finally (3) by the sum of a Lorentzian plus a Lorentzian squared. The quality of the fit parameter ( $\chi$ ) for  $x=0.65$  over the whole temperature range and for  $x=0.70$  near  $T_C$  resulting from fits to the above three dependences are pictured in Figs. 10(a) and 11(a). These results are in agreement with the above qualitative description of the temperature evolution of the  $q$  dependence of the scattering and confirm the occurrence of three regimes of SANS.

(1)  $T > T_C$ . The lineshape is Lorentzian and the Ornstein-Zernike law is satisfied. The two parameters of the fit:  $A$  and  $\kappa^2$  are pictured in Figs. 10(b), 10(c), and 11(b), 11(c).  $A$  is relatively temperature independent and  $\kappa^2$  tends to zero at  $T_C$ . The  $T$  dependence of these parameters is that expected from a standard mean field ferromagnet.<sup>35,36</sup>

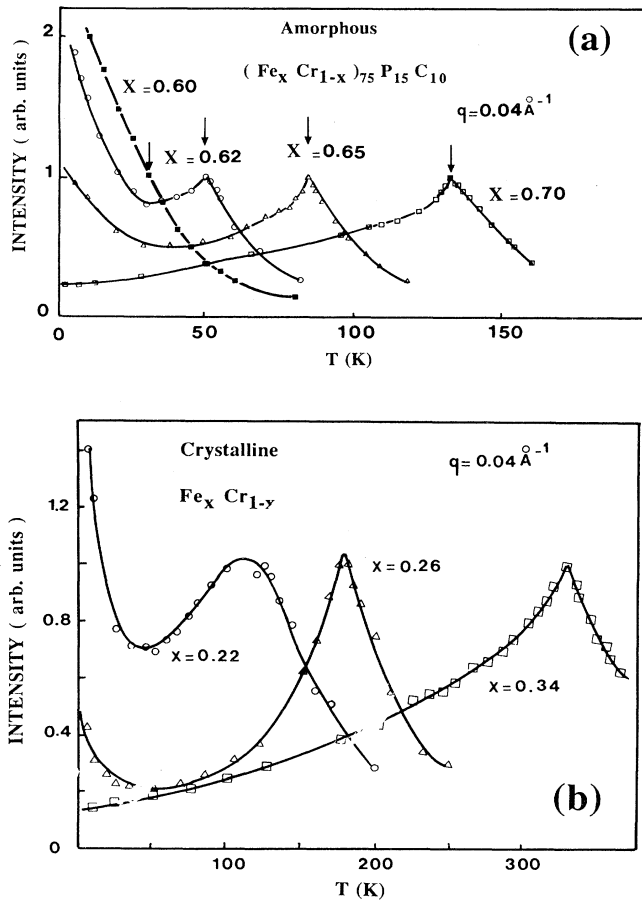


FIG. 8. Thermal dependence of the small-angle neutron scattering at  $q=0.04 \text{ \AA}^{-1}$  from amorphous  $(\text{Fe}_x \text{Cr}_{1-x})_{75} \text{P}_{15} \text{C}_{10}$  (a) and crystalline  $\text{Fe}_x \text{Cr}_{1-x}$  (b) alloys. The arrows in Fig. 8(a) correspond to  $T_C$  as determined from the Mössbauer spectra. The intensities are normalized to 1 at  $T_C$ .

(2)  $T < T_C$ . The sum of two Lorentzians representing longitudinal and transverse spin fluctuations give a quite satisfactory fit with two distinct correlation lengths:  $1/\kappa_{\parallel}$  and  $1/\kappa_{\perp}$ . The second Lorentzian contribution is consistent with the onset of the downward curvature of the  $1/I$  versus  $q^2$  data seen at low  $q$ . The  $\kappa^2$  of the Lorentzian associated with the transverse fluctuation was zero ( $< 10^{-8}$ ) and that corresponding to the longitudinal fluctuations increased sharply below  $T_C$ . The amplitude  $A_{\perp}$  was approximately twice  $A_{\parallel}$ . Figures 10(b), 10(c), 11(b), and 11(c) show  $A_{\parallel}$ ,  $A_{\perp}$ ,  $K_{\parallel}^2$ , and  $K_{\perp}^2$ . As shown in these figures  $A_{\parallel} + A_{\perp} \simeq A$ , the coefficient of the single Lorentzian above  $T_C$ . Also displayed in these figures is the coefficient from a single Lorentzian fit and the associated  $\kappa^2$  below  $T_C$ . The  $A$  coefficient is quite similar to that obtained above  $T_C$  but  $\kappa^2$  first increases below  $T_C$ , and then decreases as  $T$  decreases and finally reaches 0 at about 50 K for the  $(\text{Fe}_{0.65} \text{Cr}_{0.35})_{75} \text{P}_{15} \text{C}_{10}$  alloy. It can be noted that such a  $\kappa^2$  behavior is similar to that observed by Aeppli *et al.* in the  $(\text{Fe}_x \text{Mn}_{1-x})\text{-P-B-Al}$ .<sup>17</sup> In our sample this  $\kappa^2$  variation is an artifact due to the one-Lorentzian fit. The two Lorentzians fit is clearly the more valid and physically realistic. It proves that there is a break of the isotropic symmetry at  $T_C$ , which is the qualitative signature of the second-order paramagnetic to

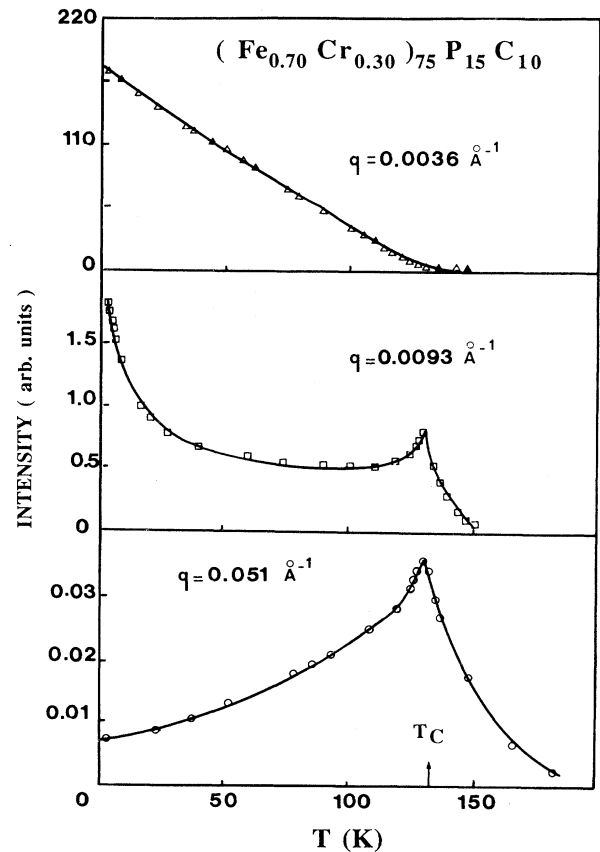


FIG. 9. Thermal dependence of the small-angle neutron scattering from the  $(\text{Fe}_{0.70} \text{Cr}_{0.30})_{75} \text{P}_{15} \text{C}_{10}$  amorphous alloys at three different  $q$  values.

ferromagnetic transition. The second signature is the fact that the correlation length ( $1/\kappa$ ) diverges both from above (paramagnetic fluctuations) and from below (longitudinal fluctuations)  $T_C$ .  $\kappa^2$  for  $T > T_C$  and  $\kappa_{\parallel}^2$  for  $T < T_C$  are approximately linear in  $|T - T_C|$  with a larger slope below  $T_C$  as expected from the mean-field approximation. Finally as expected for the transverse susceptibility of an isotropic ferromagnet  $K_{\perp}^2 = 0$ .

We strongly emphasize that the temperature dependence of these parameters near  $T_C$  is in accordance with the occurrence of a standard paramagnetic-ferromagnetic transition, at least as far as revealed by SANS in the  $0.01 < q < 0.1 \text{ \AA}^{-1}$  range (i.e., corresponding to the 50–500  $\text{\AA}$  length scale).

At low temperatures, the sum of a Lorentzian and a Lorentzian-squared cross section has to be introduced to fit the upward curvature data. As shown in Figs. 10 and 12, both the Lorentzian and Lorentzian-squared coefficients increase as  $T$  decreases. At the lower temperatures,  $\kappa^2$  becomes nonzero for  $x=0.65$  and the correlation length is at the limit of the instrumental resolution and can be estimated to be 400–600  $\text{\AA}$ . However  $\kappa^2$  remains practically zero for  $x=0.70$ .

#### D. Analysis of the data for $x = 0.62$

As in the previous samples, a good fit of the data was achieved above  $T_C$  (well defined by the peak in the CS) by

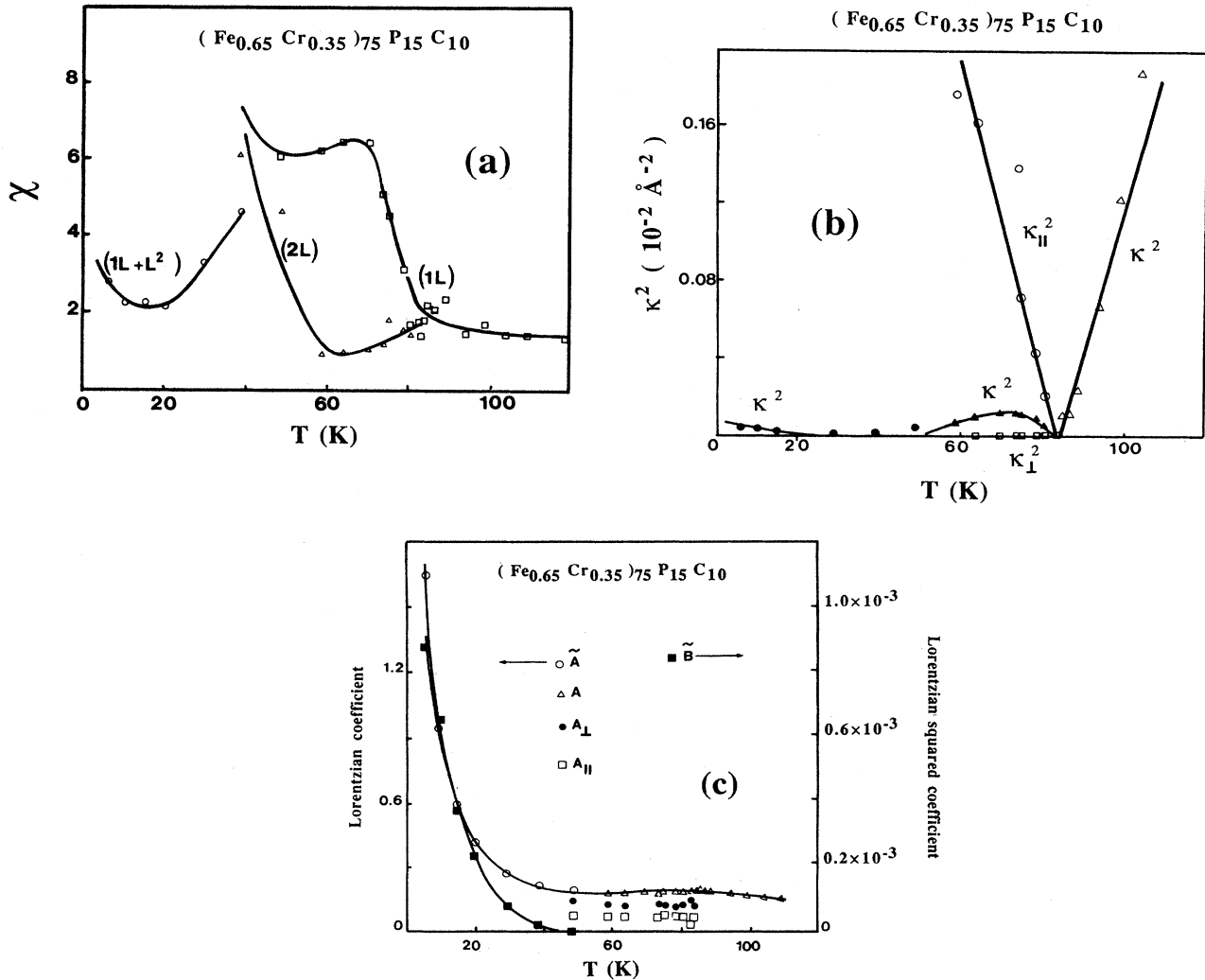


FIG. 10. (a) Comparison of the  $\chi$  resulting from the different fitting procedures, one Lorentzian (1L), two Lorentzians (2L), one Lorentzian + Lorentzian-squared ( $1L + L^2$ ) of the  $(\text{Fe}_{0.65}\text{Cr}_{0.35})_{75}\text{P}_{15}\text{C}_{10}$  amorphous alloys over the entire temperature range. (b) Thermal dependence of the inverse square of the correlation lengths as determined by the fitting procedure.  $\kappa^2$  near  $T_C$  (above and below) in the (1L) fit.  $\kappa_{\parallel}^2$  and  $\kappa_{\perp}^2$  below  $T_C$  in the (2L) fit, and  $\kappa^2$  at low temperature in the ( $1L + 1L^2$ ) fit. (c) Thermal dependence of  $A$ ,  $A_{\parallel}$ ,  $A_{\perp}$ ,  $\tilde{A}$ ,  $\tilde{B}$ , as obtained from the fitting procedure  $A$  coefficient of (1L) fit above and below  $T_C$  and  $A_{\parallel}$ , and  $A_{\perp}$  coefficients of the Lorentzians in the (2L) procedure below  $T_C$  and  $\tilde{A}$ ,  $\tilde{B}$  coefficients of the Lorentzian and the Lorentzian squared at low temperature.

a single Lorentzian and below 40 K by the sum of a Lorentzian and a Lorentzian squared [Fig. 13(a)]. In contrast to the previous samples, there was no temperature range below  $T_C$  in which the sum of two Lorentzians provided a better fit than one Lorentzian. At  $T_C$ ,  $\kappa^2$  does not reach zero. It increases slightly with decreasing  $T$  and then approaches 0 at 30 K.

The similarity between the behavior of  $\kappa^2$  in this sample below  $T_C$  and that obtained from a single Lorentzian fit in the  $x=0.65$  and  $0.70$  suggests that both longitudinal and transversal fluctuation (Fig. 13) components exist but cannot be resolved. As in a previous sample,  $A$  does not

depend very much on the temperature near  $T_C$  and is continuous with  $\tilde{A}$  at low temperatures.  $\tilde{A}$  increases dramatically at very low temperature as does  $\tilde{B}$  (Fig. 14). The correlation length also decreases at low  $T$  and becomes 200 Å at 15 K and about 100 Å at 1.5 K.

#### E. Analysis of the data for $x=0.60$

As shown in Fig. 15, the  $1/I$  versus  $q^2$  curves are parallel straight lines above 30 K and increasingly curved lines below 20 K. The onset of magnetic order is near 30 K where straight lines depart from parallelism with the

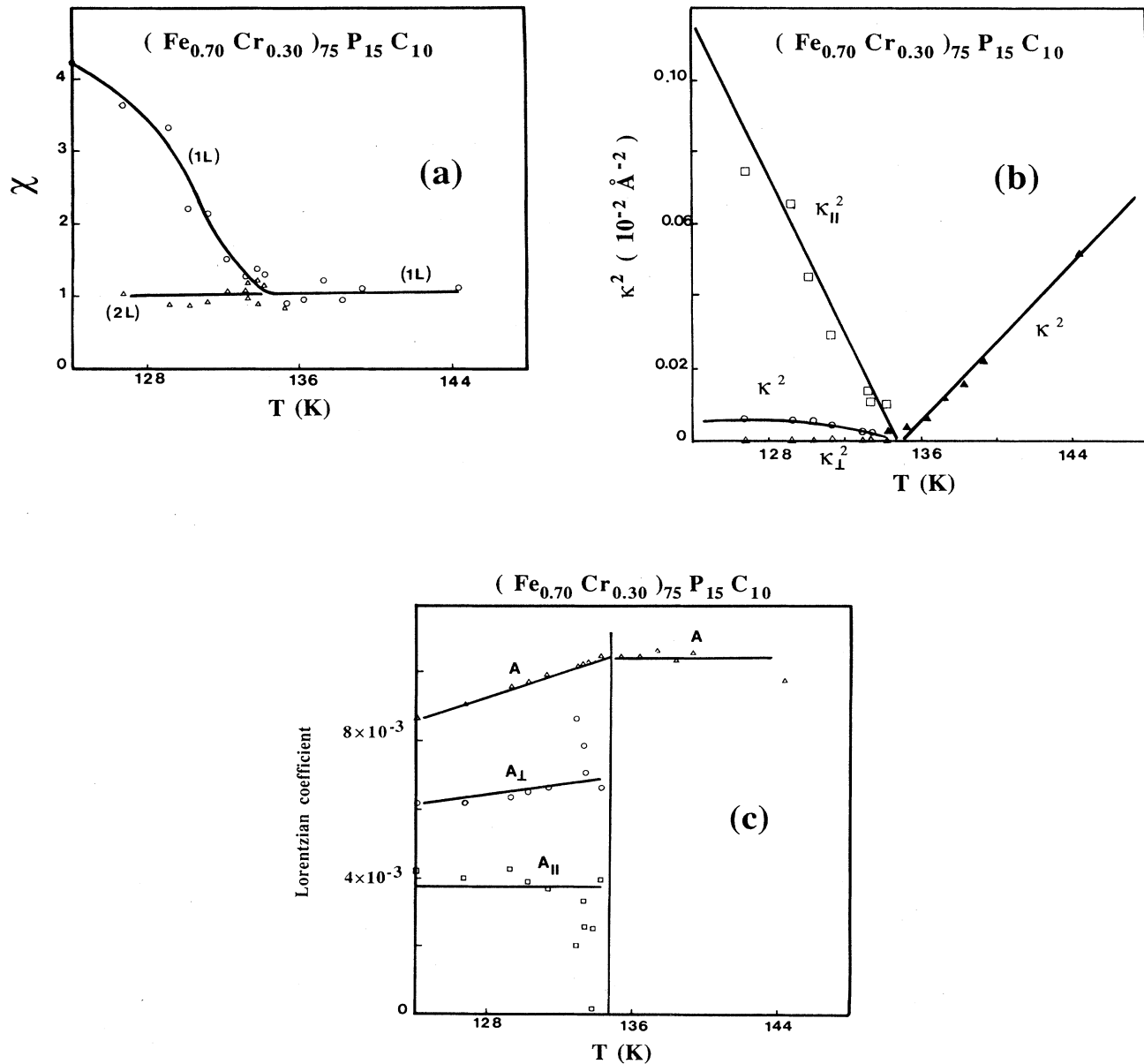


FIG. 11. (a) Comparison of the  $\chi$  resulting from the (1L) and (2L) fitting procedure near  $T_C$  in the  $(\text{Fe}_{0.70}\text{Cr}_{0.30})_{75}\text{P}_{15}\text{C}_{10}$  amorphous alloy. (b) Thermal dependence of the inverse square of the correlation lengths near  $T_C$ ,  $\kappa^2(1L)$ ,  $\kappa_{\parallel}^2$  and  $\kappa_{\perp}^2(2L)$ . (c) Thermal dependence of the Lorentzian coefficients  $A(1L)$ ,  $A_{\parallel}$  and  $A_{\perp}(2L)$  near  $T_C$ .

high-temperature data and where the Mössbauer spectroscopy shows the occurrence of a hyperfine field. The best fit was achieved by a single Lorentzian for  $T \gtrsim 25$  K and the sum of a Lorentzian and a Lorentzian squared at lower temperatures. As in the previous samples,  $\tilde{A} \simeq A$  and increases dramatically at low temperatures with  $\tilde{B}$  [Fig. 16(b)]. In this sample however,  $\kappa^2$  never reaches 0. The correlation length [Fig. 16(a)] increases to  $70 \text{ \AA}$  near 25 K. At low temperature it decreases to  $35 \text{ \AA}$  concurrent with the increase in  $\tilde{A}$  and  $\tilde{B}$ .

#### F. Very low- $q$ measurements and irreversibilities in SANS

As seen in Fig. 9, when the data are collected at very low  $q$ , a peak in the critical scattering at  $T_C$  is not found even for the most iron concentrated sample. In fact, at the lowest  $q$  we observe the tail of the forward scattering peak, the intensity of which is proportional to the square of the order parameter and the width of which is approximately the inverse of the size of the domains. Since this tail extends out beyond  $q = 3 \times 10^{-3} \text{ \AA}^{-1}$ , it means the size of the domains is of the order of some thousands of  $\text{\AA}$ . It is very difficult to tell from the data if there is a change of the size of the domains with temperature, because the change of intensity can come from a change of the size of the domains and from the order parameter inside the domains. Moreover, the data were difficult to fit with confidence because the instrumental resolution is quite important at these small scattering angles.

To see the effect of the thermal history of the sample, a 1000 Oe magnetic field was applied on the  $(\text{Fe}_{0.65}\text{Cr}_{0.35})_{75}\text{P}_{15}\text{C}_{10}$  sample above  $T_C$  and then the sample was cooled to 1.5 K. At this temperature the field

was removed and the “after-field-cooled” (AFC) data were collected on heating the sample. The first observation was that scattering was practically 0 when the field was applied. The second observation was the AFC scattering was very different from the scattering from the sample cooled under zero field (Fig. 17). As shown previously,<sup>19</sup> the correlation length is smaller in the AFC state just after the switching off of the field and increases with the temperature. The  $\xi$  values in Ref. 19 have to be considered as approximate as seen from the standard deviation values.

A more accurate study of the effect of the thermal history of the sample has been carried out in the  $x=0.62$  sample in the  $0.01 < q < 0.1 \text{ \AA}^{-1}$  range with a convergent beam collimation system on the SANS spectrometer at the National Institute of Standards and Technology (NIST). The experiment was the same as the previous one and the data are qualitatively similar. The scattering is very small with a field applied and at first increases irreversibly after switching off the field. The fit of the data showed, however, that the coefficient of the Lorentzian,  $\tilde{A}$ , was independent of the thermal history of the sample. The irreversibilities are evident only in the Lorentzian-squared coefficient  $\tilde{B}$  [Fig. 14(b)] and in the correlation length [Figure 13(b)]. As already shown for the  $(\text{Fe}_{0.65}\text{Cr}_{0.35})_{75}\text{P}_{15}\text{C}_{10}$  sample, in the  $0.003 < q < 0.01 \text{ \AA}^{-1}$  range,<sup>19</sup> the correlation length is smaller at low temperature in the AFC state.

These data suggest that the external field aligns the domains and makes the scattering disappear into the forward beam. At low temperatures, only small domains, which need a smaller thermal energy to move, are formed. Their size increases as the thermal energy allows them to cross barriers.

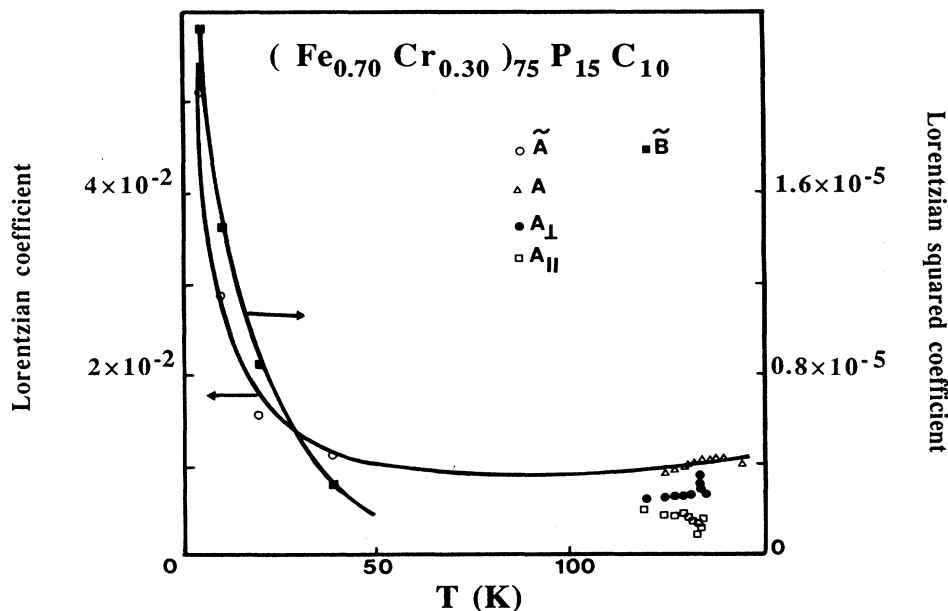


FIG. 12, Thermal dependence of the  $\tilde{B}$  and  $\tilde{A}$  coefficients in the  $(1L + 1L^2)$  fit.  $A$ ,  $A_{\parallel}$ , and  $A_{\perp}$  near  $T_C$  are the values of Fig. 11 in the  $(\text{Fe}_{0.70}\text{Cr}_{0.30})_{75}\text{P}_{15}\text{C}_{10}$  sample.

IV. INELASTIC SCATTERING

A. Background

By using a triple-axis spectrometer,<sup>40</sup> we can measure the magnetic excitations in these alloys below  $T_C$ . The scattering intensity is proportional to the convolution of the cross section with the instrumental resolution. The spin-wave cross section representing the space and time Fourier transform of the two spin correlation function can be expressed as

$$I(q, E) = \frac{d_\sigma^2}{d\Omega dE} = A_D \frac{k_F}{k_I} \frac{E}{1 - \exp(-E/k_B T)} \frac{F(q, E)}{q^2},$$

where  $A_D$  should be constant for an ideal ferromagnet and  $F(q, E)$  is the spectral weight function.  $F(q, E)$  can

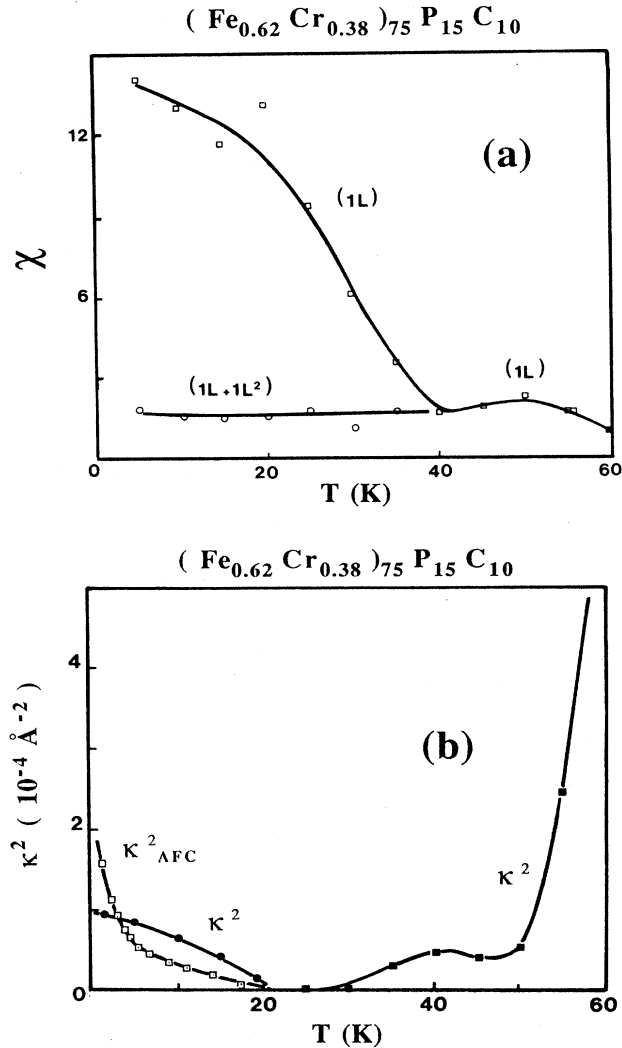


FIG. 13. (a) Comparison of the  $\chi$  resulting from (1L) and (1L + 1L<sup>2</sup>) fit in the (Fe<sub>0.62</sub>Cr<sub>0.38</sub>)<sub>75</sub>P<sub>15</sub>C<sub>10</sub> amorphous alloy. (b) Thermal dependence of the inverse of the square of the correlation length resulting from the 1L fit above 40 K and the (1L + 1L<sup>2</sup>) fit below 40 K.  $\kappa_{AFC}^2$  is the inverse of the correlation length found in the AFC state resulting from a (1L + 1L<sup>2</sup>) fit.

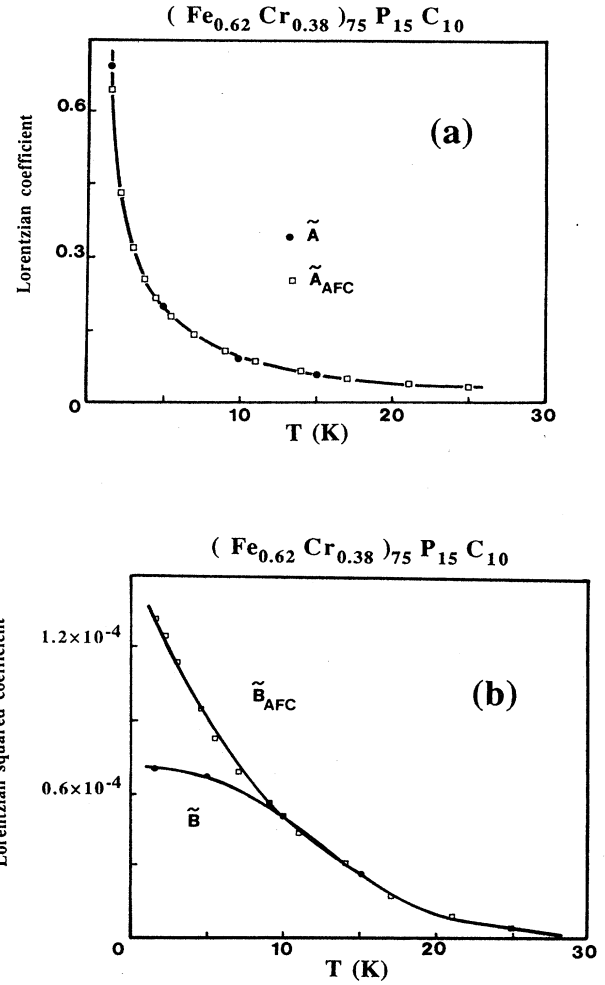


FIG. 14. Thermal dependence of  $\tilde{A}$  (a) and  $\tilde{B}$  (b) in the zero field and the AFC states.

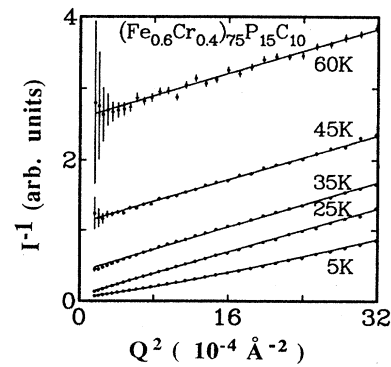


FIG. 15.  $I^{-1}$  as a function of  $q^2$  for the SANS from the (Fe<sub>0.60</sub>Cr<sub>0.40</sub>)<sub>75</sub>P<sub>15</sub>C<sub>10</sub> amorphous alloy.

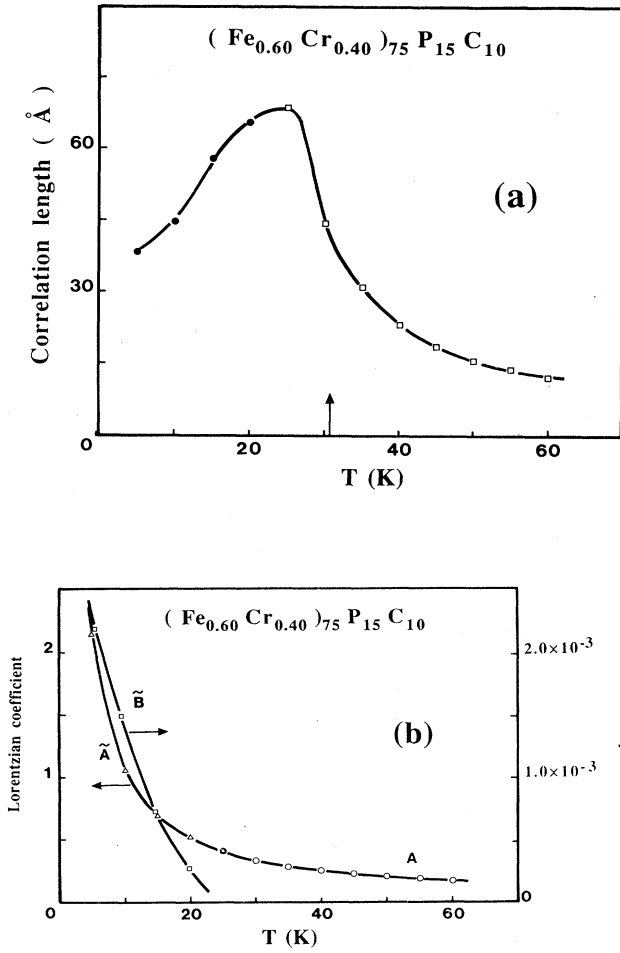


FIG. 16. (a) Thermal dependence of the correlation length in the  $(\text{Fe}_{0.60}\text{Cr}_{0.40})_{75}\text{P}_{15}\text{C}_{10}$  amorphous alloy.  $1L$  was used for  $T > 25$  K ( $\square$ ), and  $(1L + 1L^2)$  for  $T < 25$  K ( $\odot$ ). The arrow indicates the Curie temperature obtained from the hyperfine field. (b) Thermal dependence of the coefficients ( $A$ ) in the  $1L$  ( $\odot$ ) and  $\bar{A}$  ( $\triangle$ ) and  $\bar{B}$  ( $\square$ ) in the  $(1L + 1L^2)$  fit.

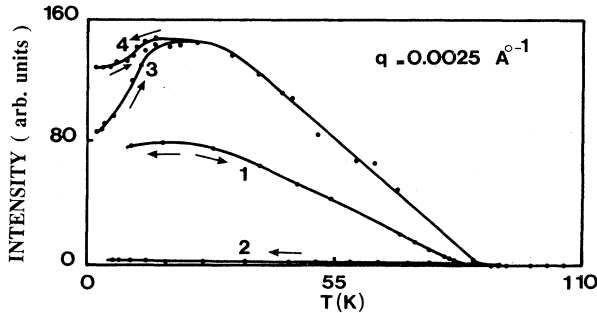


FIG. 17. Example of the evolution of the SANS at  $q = 0.0025$   $\text{\AA}^{-1}$  from the  $(\text{Fe}_{0.65}\text{Cr}_{0.35})_{75}\text{P}_{15}\text{C}_{10}$  amorphous alloy in zero field (1), under 1000 Oe (2), and in the AFC states 3 and 4.

be chosen as a double Lorentzian<sup>40,15</sup> or alternatively as a damped harmonic oscillator.<sup>21,41</sup> The choice between these two functions has been debated. It has been shown that they give equivalent results for the small damping limit. In the analysis, we present the double-Lorentzian (DL) and damped-harmonic-oscillator (DHO) fits

$$\text{(DL)} \quad F(q, E) = (1/\pi) \{ \Gamma_q / [(E - E_q)^2 + \Gamma_q^2] + \Gamma_q / [(E + E_q)^2 + \Gamma_q^2] \},$$

$$\text{(DHO)} \quad F(q, E) = (1/\pi) \{ 2\Gamma_q E_q^2 / [(E - E_q)^2 + 4E^2 \Gamma_q^2] \},$$

where  $\Gamma_q$  is the half-width of the excitation (for small  $\Gamma_q/E_q$ ) and  $E_q$  its energy. The two terms in the DL function correspond to the annihilation and the creation process for spin excitations. In a ferromagnet for small  $q$ ,  $E_q$  can be written as  $Dq^2 + \Delta$ , where  $D$  is the stiffness of the spin waves and  $\Delta$  is pseudo-dipolar gap term that is generally very small.<sup>17</sup> The thermal dependence of  $D(T)$  and  $\Gamma(T)$  are conventionally

$$D(T) = D_0 [1 - A_0 (T/T_C)^{5/2}] \quad \text{for } T \ll T_C$$

and

$$\Gamma(T) = \Gamma(0) T^2 q^4 \ln^2(kT/E_q) \quad \text{for } E_q \ll kT.$$

For a standard ferromagnet  $D(T)$  increases with the order parameter (the spontaneous magnetization) when the temperature is lowered.  $\Gamma(T)$  decreases when  $T$  is lowered as the result of the smaller probability of two-magnon interactions. As tabulated by Rhyne,<sup>25</sup> the ratio between the stiffness and  $T_C$  is close to 2.25 in most amorphous magnetic alloys.

The experiments must all be done at small  $q$  near the (000) forward peak which is the only sharp scattering peak of an amorphous structure. This requires relatively good energy resolution for alloys of low  $T_C$ . The experimental conditions used in this study for the amorphous alloys were chosen as a compromise between the resolution of the instrument, the intensity, and the available range of energy transfer. Using a triple-axis instrument at NIST with an incident energy of 3.75 meV and collimation of  $20' - 20' - 20' - 20'$ , the resolution was 0.029 meV half width at half maximum. However, to reach this resolution, intensity was sacrificed so that the counting time was 1 day per scan for the lowest temperatures.

Due to the reduced intensity under these tight resolution conditions the inelastic scattering was not studied as a function of  $q$ . Data were collected only for  $q = 0.07$   $\text{\AA}^{-1}$  which is the smallest  $q$  for which the spin-wave scattering could be clearly separated from the elastic peak. We then assumed  $\Delta = 0$  and the validity of the  $E = Dq^2$  law. Within these experimental restrictions, we could measure the variation of the spin waves in  $x = 0.70$ ,  $x = 0.725$ , and  $x = 0.75$  samples. These alloys are thus richer in iron compared to those studied by low-field magnetic measurement and SANS.

## B. Experimental data

Representative spectra collected for  $x = 0.70$  and  $x = 0.75$  are pictured in Fig. 18. For  $x = 0.75$ , the

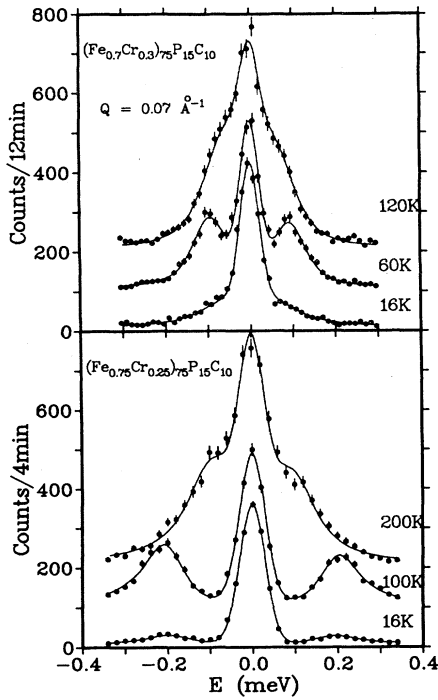


FIG. 18. Inelastic neutron spectra collected from the  $(\text{Fe}_{0.7}\text{Cr}_{0.3})_{75}\text{P}_{15}\text{C}_{10}$  and  $(\text{Fe}_{0.75}\text{Cr}_{0.25})_{75}\text{P}_{15}\text{C}_{10}$  amorphous samples.

creation and annihilation peaks are very well resolved down to 12 K. The shift of their position to larger  $|E|$  is clearly observed from  $T_C$  down to 60 K. Below this temperature their position appears rather constant and the peak width tends to increase. For  $x=0.70$  the creation and annihilation peaks are well resolved near 60 K. But below this temperature, they shift towards the central peak (comprised largely of elastic scattering from cryostat and sample holder). At the same time, their width increases strongly and they are less and less well resolved, as shown in Fig. 18 for  $x=0.70$ . At low temperature  $\Gamma_q/E_q \approx 1$  and there is an approximate critical damping of the spin waves.

Figure 19 shows the temperature dependence of  $E_q$  and  $\Gamma_q$  in the  $(\text{Fe}_{0.70}\text{Cr}_{0.30})_{75}\text{P}_{15}\text{C}_{10}$  sample for the DL and DHO fits. In both cases  $\Gamma_q$  reaches a minimum with decreasing temperature as observed for most reentrant-spin-glass systems. The behavior of  $E_q$  is different, however, for the two types of fits. For the DL fit  $E_q$  reaches a maximum with decreasing temperature which again is typical for reentrant-spin-glass behavior. The maximum in  $E_q$  occurs at roughly the temperature of the minimum in  $\Gamma_q$ . However,  $E_q$  from the DHO fit continues to increase as the temperature is decreased. There is a hint of a minimum in  $E_q$  at about 40 K as observed by Hennion *et al.* in  $\text{Ni}_x\text{Mn}_{1-x}$ .<sup>22</sup> The recent paper of Lequien *et al.*<sup>45</sup> found no such minimum in crystalline  $\text{Fe}_x\text{Cr}_{1-x}$ . Note that  $E_q$  from the DHO fit does not renormalize properly towards zero as  $T_C$  is approached. Here the DHO model clearly gives unphysical results for our data. The discrepancy at low temperature between the DL and

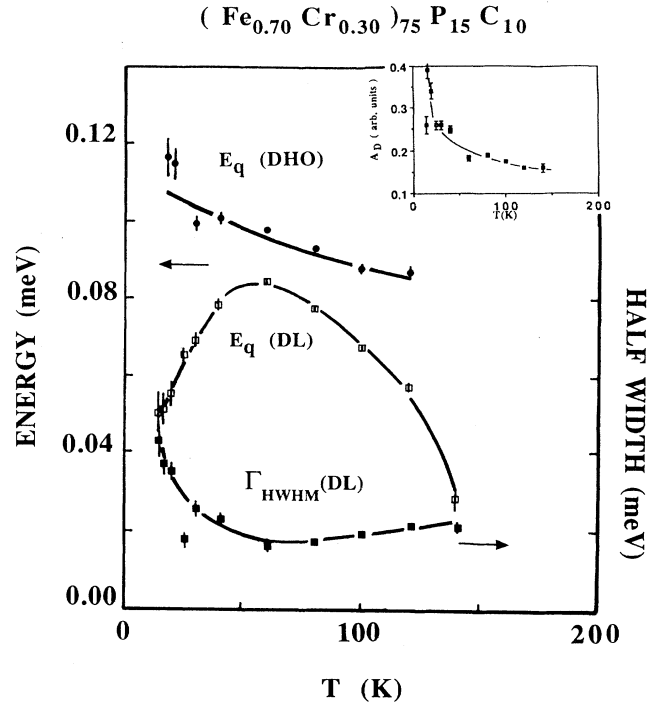


FIG. 19. The temperature dependence of the spin-wave energy and the half width as obtained from fits by a double Lorentzian (DL) and the damped harmonic oscillator (DHO) models for  $q=0.07 \text{ \AA}^{-1}$ .

DHO fits is explained by the fact that  $E_q$  for the DHO model does not correspond to the excitation frequency.<sup>24</sup> The excitation frequency is less than  $E_q$  in this model due to the increased damping at low temperatures. This increased damping arises from the spin-glass structure and is not a thermal population effect as observed near  $T_C$ . In the inset of Fig. 19, we observe that  $A_D$  (which theoretically should be independent of the temperature) increases below 40 K, as does the Lorentzian term in the SANS.

The  $T$  dependence of  $D/kT_C$  versus  $T/T_C$  obtained from the DL fit for the  $(\text{Fe}_x\text{Cr}_{1-x})_{75}\text{P}_{15}\text{C}_{10}$  alloys and for the  $\text{Fe}_x\text{Cr}_{1-x}$  crystalline counterpart<sup>20</sup> shows behavior very similar to that obtained by Erwin *et al.*<sup>3,23</sup> in the  $(\text{Fe}_x\text{Ni}_{1-x})_{75}\text{P}_{16}\text{B}_6\text{Al}_3$  system, but the occurrence of an envelope is not so clear. The comparison between data obtained from crystalline and amorphous  $(\text{Fe}_x\text{Cr}_{1-x})$  alloys are close when they have the same Curie temperature. The data can be compared to those obtained by Xianyu<sup>42</sup> for the  $(\text{Fe}_{87.5}\text{Cr}_{12.5})_{80}\text{P}_{13}\text{C}_7$ , by Wicksted<sup>43</sup> for the  $(\text{Fe}_{77}\text{Cr}_{23})_{75}\text{P}_{16}\text{B}_6\text{Al}_3$  and  $\text{Fe}_{75}\text{P}_{15}\text{C}_{10}$  alloys.<sup>40</sup> The data of Refs. 42 and 43 are qualitatively those expected from the  $T_C$ , but with a smaller  $D$ . On the contrary,  $D$  in Ref. 40 is large and  $D/kT_C$  reaches 2.89 for  $T/T_C=0.495$ . Recall that for pure iron  $D/kT_C=3.12$ .<sup>44</sup>

Finally, although we obtain an increase in  $D$  at low temperature in the DHO fit similar to that given by Hennion *et al.* in  $\text{Ni}_x\text{Mn}_{1-x}$ ,<sup>22</sup> we do not have confidence in this result. The DHO fit clearly fails near  $T_C$  and it is

not clear that the  $D$  derived from this model is physical. This is in agreement with the very recent paper of Lequien *et al.*<sup>45</sup> who also did not observe any increase in crystalline  $\text{Fe}_x\text{Cr}_{1-x}$  in a reinvestigation of the  $\text{Fe}_{26}\text{Cr}_{74}$  sample used previously by Shapiro *et al.*<sup>20</sup>

## V. CONCLUSIONS

The  $(\text{Fe}_x\text{Cr}_{1-x})_{75}\text{P}_{15}\text{C}_{10}$  system exhibits the now classical experimental features of a reentrant spin glass near the multicritical point. This paper presents further information on three points (i) the behavior of the alloys near  $T_C$  (both above and below), (ii) the different stages of the onset of spin-glass order from paramagnetism have been defined clearly using a number of different experimental techniques, and (iii) a comparison can be made between crystalline  $\text{Fe}_x\text{Cr}_{1-x}$  alloys and their amorphous counterparts.

Recently, the occurrence of a magnetic transition at  $T_C$  and then the nature of the paramagnetic-ferromagnetic transition in RSG was questioned.<sup>46</sup> Our first conclusion is that there is a paramagnetic-ferromagnetic transition in the  $(\text{Fe}_x\text{Cr}_{1-x})_{75}\text{P}_{15}\text{C}_{10}$  amorphous alloy and it is practically standard for  $T_C > 50$  K.

Mössbauer spectroscopy shows the thermal average of the spins increases from 0 above  $T_C$  to a finite value below  $T_C$ . That does not prove the spins become parallel but it indicates that an order parameter increases from 0 in the magnetic phase.

The field magnetic measurements carried out in adequate field and geometry conditions ( $H/N$  small) shows that at this same temperature, the susceptibility becomes very large. The spins tend to become parallel very easily, as expected for a paramagnetic-ferromagnetic transition.

SANS above  $T_C$  exhibits the features expected for magnetic fluctuations in a paramagnetic phase preceding a ferromagnetic transition: SANS follows the Ornstein-Zernike law with a correlation length increasing as  $T$  is closer to  $T_C$ . A peak in the critical scattering is observed at  $T_C$ .

Below  $T_C$ , the dynamic fluctuations are consistent with a breaking of the isotropical symmetry as expected from the paramagnetic-ferromagnetic transition. Transverse fluctuations with infinite correlation length and longitudinal fluctuations with decreasing correlation length have to be introduced to fit the data.

The spin waves (measured in samples whose  $T_C$  is larger than 134 K) exhibit an increase of the stiffness and a decrease of the width as expected from a ferromagnet in a significant temperature range below  $T_C$ .

The only limitation to a standard ferromagnetic phase is the size of the domains below  $T_C$ . They reach certainly no more than a few thousand Å and this size decreases with the Curie temperature. However they can grow (or be aligned) very easily in small fields.

The second conclusion is that, as in similar frustrated systems, the ferromagnetism tends to be destroyed as the temperature is lowered. The breaking of the ferromagnetism can be described in three stages corresponding to different behaviors in magnetization, SANS, or spin waves. These stages are separated by more or less well-

defined lines at  $T^*$ ,  $T_1$ , and  $T_2$ . The temperatures are reported in the tentative phase diagram of Fig. 20 with  $T_C$  and the other "transition temperatures" observed in the  $\text{Fe}_x\text{Cr}_{1-x}$  crystalline counterpart.

The highest-temperature anomalies are observed in spin waves. In the DL fits the stiffness reaches a maximum and decreases below  $T^*$  as the width  $\Gamma$  increases. The perturbation in the dynamics of the spin waves is not seen in magnetic measurements or in SANS above  $T_1$ .  $T_1$  is the temperature at which  $\sigma_{\text{FC}}$ , when it is close to the spontaneous magnetization ( $H$  small,  $H/N$  large), reaches a maximum.  $T_1$  is also approximately the temperature below which a Lorentzian-squared contribution has to be introduced to fit the SANS data. Thus below this temperature, there is likely a small decrease of the spontaneous magnetization due to a collective phenomena but without strong irreversibilities nor significant decrease of the correlation length.

The strong irreversibilities and the significant decrease of the correlation lengths take place only at  $T_2$ :  $\sigma_{\text{ZFC}}$  separates from  $\sigma_{\text{FC}}$ , the coercive field increases and the SANS depends significantly on the thermal history of the sample—the correlation length increases to 100 Å for  $x = 0.62$  and to about 250 Å for  $x = 0.65$ . The coefficient of the Lorentzian and of the Lorentzian-squared increase abruptly. It is to be noted that these temperatures are approximate because when we see the maximum of  $D$  or

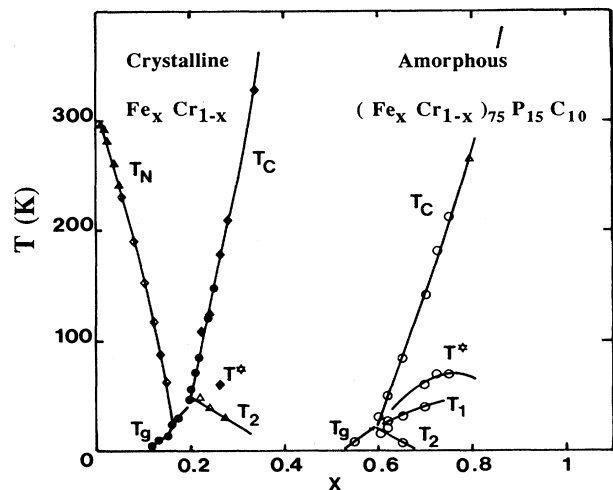


FIG. 20. Magnetic phase diagram of the  $(\text{Fe}_x\text{Cr}_{1-x})_{75}\text{P}_{15}\text{C}_{10}$  amorphous alloy and of the  $\text{Fe}_x\text{Cr}_{1-x}$  crystalline alloy ( $\circ$ : this work).  $T_C$ : Curie temperature.<sup>14,20</sup>  $T_g$ : temperature of the maximum of susceptibility in the ferromagnetic-spin-glass transition.<sup>47</sup>  $T_1$ : temperature of the maximum of the zero-field-cooled magnetization below this temperature the coefficient of the Lorentzian-squared term in the SANS cross section becomes significant.  $T_2$ : Temperature below which strong irreversibilities occur in the ferromagnetic phase.  $T^*$ : Temperature below which the stiffness of the spin waves decrease.<sup>15,20</sup>  $T_N$ : Néel temperature of the antiferromagnet crystalline  $\text{Fe}_x\text{Cr}_{1-x}$  (Refs. 48 and 49).

$\sigma_{FC}$ , the departures from standard ferromagnetic behavior have already taken place at a higher temperature.

The comparison between our phase diagram and that proposed by Gabay and Toulouse is not straightforward. Possibly, the temperature  $T_2$  could correspond to the  $M_1 \rightarrow M_2$  transition, which is consistent with the onset of strong irreversibilities.  $T_1$  could correspond to the extreme in the  $M_1$  phase. The small canting of spins would

decrease  $\sigma_{FC}$  and it has been suggested that this might also contribute to the Lorentzian-squared contribution of SANS.<sup>41</sup>

The sample  $x=0.60$  is very close to the multicritical point. It exhibits some important feature of the paramagnetic-ferromagnetic transition. At 30 K the hyperfine field increases from 0 and in very low field, the low-field demagnetization plateau is reached. Above 30 K, the magnetic fluctuations are those preceding a paramagnetic-ferromagnetic transition. But this time the correlation length does not exceed 70 Å at  $T_C$  and between 25 and 30 K. This correlation length is smaller than that reached by the  $(\text{Fe}_{0.65}\text{Cr}_{0.35})_{75}\text{P}_{15}\text{C}_{10}$  alloy in the RSG temperature range. So if we considered only the correlation length, we would say the  $x=0.60$  sample becomes directly a spin glass. Contrary to what happens at low temperature for samples with a larger correlation length, the 70 Å size domains of the  $x=0.60$  sample can be very easily aligned under an external magnetic field in the 25–30 K temperature range. The domains freeze only below 25 K as their size decrease to reach finally 17 Å at 5 K.

In Fig. 20, the phase diagrams of the amorphous system and of the  $\text{Fe}_x\text{Cr}_{1-x}$  crystalline counterpart are compared. The most obvious difference between the two is the shift of the multicritical point from  $x=0.2$  to  $x=0.6$ . Such a difference comes partly from the addition of metalloid atoms in the amorphous system. However, even if we write the family of the  $x=0.6$  system  $\text{Fe}_{0.45}\text{M}_{0.55}$  ( $M=\text{P},\text{C},\text{Cr}$ ) the relative concentration of iron in the amorphous system at the multicritical concentration is still twice that of the crystalline system. This illustrates the role played by the amorphous structure as discussed by Boliang *et al.*<sup>30</sup> It is noted that the Curie temperatures of the amorphous and crystalline systems also vary in a parallel fashion.

The neutron scattering data show a remarkable similarity between amorphous and crystalline alloys having the same Curie temperature. As seen in Fig. 8, the relative proportion of critical scattering and subcritical scattering are very similar when the Curie temperatures are close. In Fig. 21, the  $\text{Fe}_{0.26}\text{Cr}_{0.74}$  crystalline sample whose Curie temperature is 178 K is between that of the amorphous alloys whose Curie temperatures are 134 and 181 K. It is thus apparent that for the Fe-Cr system, the occurrence of reentrant phenomena is closely linked to the magnitude of the Curie temperature. If the Curie temperature is related to the average exchange  $\langle J \rangle$  and the driving force to reentrance to the exchange fluctuation  $\langle \Delta J \rangle$ , we suggest that for a given  $\langle J \rangle$ , the  $\langle \Delta J \rangle$  are very similar in both amorphous and crystalline systems, independent of the iron concentration.

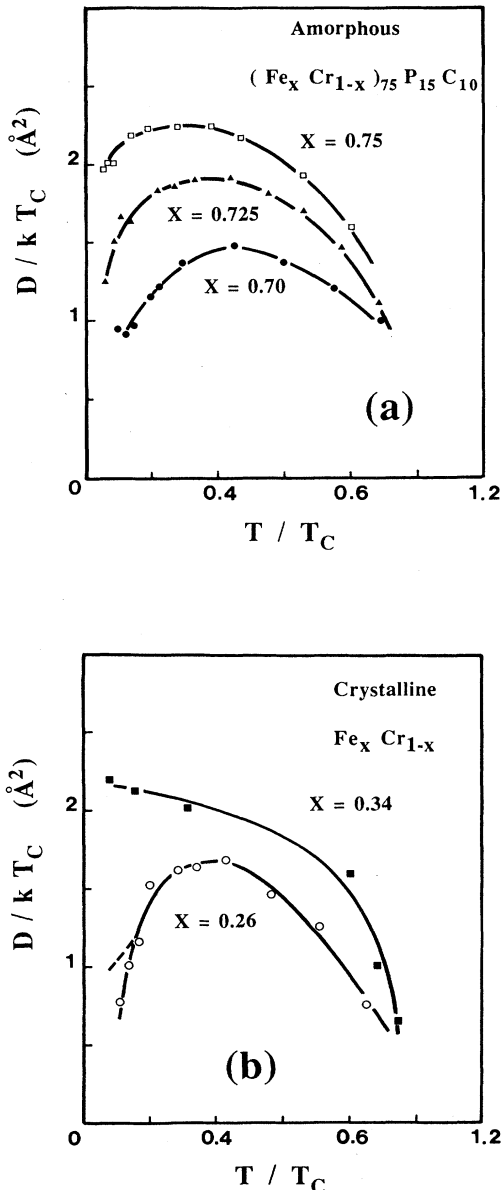


FIG. 21. Reduced temperature dependence of the spin stiffness  $D/kT_c$  for  $x=0.70$ ,  $x=0.725$ , and  $x=0.75$  in the amorphous  $(\text{Fe}_x\text{Cr}_{1-x})_{75}\text{P}_{15}\text{C}_{10}$  alloy (a), and for  $x=0.26$  and  $x=0.34$  in the crystalline  $\text{Fe}_x\text{Cr}_{1-x}$  system (b) [20] and after reinvestigation [dashed lines, Ref. 45].

#### ACKNOWLEDGMENTS

This work was financially supported by NATO for one of us (Ph.M.) to visit the National Institute of Standards and Technology (NIST).

- <sup>1</sup>For a review, see K. Moorjani and J. M. D. Coey, *Methods and Phenomena, Magnetic Glasses* (Elsevier, New York, 1984), Chap. VII.
- <sup>2</sup>J. Souletie, *J. Phys. (Paris)* **39**, C2-3 (1978).
- <sup>3</sup>R. W. Erwin, Ph.D. thesis, University of Maryland, 1985 (unpublished).
- <sup>4</sup>S. F. Edwards and P. W. Anderson, *J. Phys. F* **5**, 965 (1975).
- <sup>5</sup>D. Sherrington and S. Kirkpatrick, *Phys. Rev. Lett.* **35**, 1792 (1975); S. Kirkpatrick and D. Sherrington, *Phys. Rev. B* **17**, 4384 (1978).
- <sup>6</sup>J. R. L. de Almeida and D. J. Thouless, *J. Phys. A* **11**, 983 (1978).
- <sup>7</sup>M. Gabay and G. Toulouse, *Phys. Rev. Lett.* **47**, 201 (1981).
- <sup>8</sup>V. Canella and J. A. Mydosh, in *Magnetism and Magnetic Materials (Boston, 1973)*, Proceedings of the 19th Annual Conference on Magnetism and Magnetic Materials, AIP Conf. Proc. No. 18, edited by C. D. Graham and J. J. Rhyne (AIP, New York, 1974).
- <sup>9</sup>B. R. Coles, B. V. B. Sarkissian, and R. H. Taylor, *Philos. Mag.* **B 37**, 489 (1978).
- <sup>10</sup>S. Senoussi, *Phys. Rev. B* **31**, 6086 (1985); *Phys. Rev. Lett.* **51**, 2218 (1983).
- <sup>11</sup>S. Senoussi and D. Elkhatouri, *J. Magn. Magn. Mater.* **56**, 153 (1986).
- <sup>12</sup>W. Abdul-Razzaq and J. S. Kouvel, *J. Appl. Phys.* **57**, 3467 (1985).
- <sup>13</sup>M. A. Manheimer, S. M. Baghat, and H. S. Chen, *J. Magn. Magn. Mater.* **38**, 147 (1983).
- <sup>14</sup>S. K. Burke, R. Cywinski, J. R. Davis, and B. D. Rainford, *J. Phys. F* **13**, 441 (1983); **13**, 451 (1983); **13**, 474 (1983).
- <sup>15</sup>C. R. Fincher, S. M. Shapiro, A. H. Palumbo, and R. D. Parks, *Phys. Rev. Lett.* **45**, 474 (1980).
- <sup>16</sup>A. P. Murani, *Solid State Commun.* **34**, 750 (1980).
- <sup>17</sup>G. Aeppli, S. M. Shapiro, R. J. Birgeneau, and H. S. Chen, (a) *Phys. Rev. B* **28**, 5160 (1983); (b) **29**, 2589 (1984).
- <sup>18</sup>M. Hennion, I. Mirebeau, F. Hippert, B. Hennion, and J. Bigot, *J. Magn. Magn. Mater.* **56**, 121 (1986).
- <sup>19</sup>D. Boumazouza, C. Tete, J. Durand, Ph. Mangin, and J. L. Soubeyroux, *J. Magn. Magn. Mater.* **54-57**, 95 (1986).
- <sup>20</sup>S. M. Shapiro, C. R. Fincher, A. C. Palumbo, and R. D. Parks, *Phys. Rev. B* **24**, 6661 (1981).
- <sup>21</sup>A. P. Murani, *Phys. Rev. B* **28**, 432 (1983).
- <sup>22</sup>B. Hennion, M. Hennion, F. Hippert, and A. P. Murani, *J. Phys. F* **14**, 489 (1984).
- <sup>23</sup>J. W. Lynn, R. W. Erwin, J. J. Rhyne, and H. S. Chen, *J. Magn. Magn. Mater.* **31-36**, 1397 (1983).
- <sup>24</sup>R. W. Erwin, J. W. Lynn, J. H. Rhyne, and H. S. Chen, *J. Appl. Phys.* **57**, 3473 (1985).
- <sup>25</sup>J. J. Rhyne, *J. Non-Cryst. Solids* **76**, 129 (1985).
- <sup>26</sup>I. A. Campbell, S. Senoussi, F. Varret, J. Teillet, and A. Hamzic, *Phys. Rev. Lett.* **50**, 1615 (1983).
- <sup>27</sup>R. A. Brand, J. Lauer, and W. Keune, *Phys. Rev. B* **31**, 1630 (1985).
- <sup>28</sup>Ph. Mangin, D. Boumazouza, C. Tete, R. W. Erwin, and J. J. Rhyne, *J. Appl. Phys.* **61**, 3619 (1987).
- <sup>29</sup>D. Boumazouza, Ph. Mangin, B. George, P. Louis, R. A. Brand, J. J. Rhyne, and R. W. Erwin, *Phys. Rev. B* **39**, 749 (1989).
- <sup>30</sup>Y. Boliang, J. M. D. Coey, M. Olivier, and J. O. Strom-Olsen, *J. Appl. Phys.* **55**, 1748 (1984).
- <sup>31</sup>For a review, see C. D. Graham and T. Egami, *Ann. Rev. Mater. Sci.* **8**, 423 (1978).
- <sup>32</sup>A. T. Aldred, *Phys. Rev. B* **14**, 219 (1976).
- <sup>33</sup>G. Dublon and Y. Yeshurun, *Phys. Rev. B* **25**, 4899 (1982).
- <sup>34</sup>M. B. Salamon, K. V. Rao, and Y. Yeshurun, *J. Appl. Phys.* **52**, 1687 (1981).
- <sup>35</sup>S. W. Lovesey, *International Series of Monographs of Physics No. 72* (Clarendon, Oxford, 1984), Chap. XIII.
- <sup>36</sup>Y. A. Izyumov and R. P. Ozerov, *Magnetic Neutron Diffraction* (Plenum, New York, 1970), Chaps. II and VII.
- <sup>37</sup>P. Debye, H. R. Anderson, and H. Brumberger, *J. Appl. Phys.* **28**, 679 (1957).
- <sup>38</sup>R. S. Birgeneau, R. A. Cowley, G. Shirane, and Y. Roshizawa, *Phys. Rev. Lett.* **54**, 214 (1985).
- <sup>39</sup>A. Aharony and E. Pytte, *Phys. Rev. B* **27**, 5872 (1983).
- <sup>40</sup>J. D. Axe, L. Passell, and C. C. Tsuei, in *Magnetism and Magnetic Materials (San Francisco, 1974)*, Proceedings of the 20th Annual Conference on Magnetism and Magnetic Materials, AIP Conf. Proc. No. 24, edited by C. D. Graham, G. H. Lande, and J. J. Rhyne (AIP, New York, 1975).
- <sup>41</sup>M. Hennion, B. Hennion, I. Mirebeau, S. Lequien, and F. Hippert, *J. Appl. Phys.* **63**, 4071 (1988).
- <sup>42</sup>X. Xianyu, Y. Ishikawa, and S. Onodera, *J. Phys. Soc. Jpn.* **51**, 1799 (1982).
- <sup>43</sup>J. P. Wicksted, S. M. Shapiro, and H. S. Chen, *J. Appl. Phys.* **55**, 1697 (1984).
- <sup>44</sup>M. F. Collins, V. J. Minkiewicz, R. Nathans, L. Passell, and G. Shirane, *Phys. Rev.* **179**, 417 (1969).
- <sup>45</sup>S. Lequien, B. Hennion, and S. M. Shapiro, *Phys. Rev. B* **38**, 2669 (1988).
- <sup>46</sup>L. D. Rakers and P. A. Beck, *Phys. Rev. B* **36**, 8622 (1987).
- <sup>47</sup>Y. Ishikawa, S. Hoshino, and Y. Endoh, *J. Phys. Soc. Jpn.* **22**, 1221 (1967).
- <sup>48</sup>S. K. Burke and B. D. Rainford, *J. Phys. F* **8**, 6239 (1978).
- <sup>49</sup>Y. Yeshurun, K. V. Rao, and M. B. Salamon, *Solid State Commun.* **38**, 371 (1981).